THE ASTROPHYSICAL JOURNAL, 555:900–917, 2001 July 10

THE METAMORPHOSIS OF SN 1998bw[1]

FERDINANDO PATAT,[2] ENRICO CAPPELLARO,[3] JOHN DANZIGER,[4] PAOLO A. MAZZALI,[4,5] JESPER SOLLERMAN,[2,6] THOMAS AUGUSTEIJN,[7] JAMES BREWER,[7] VANESSA DOUBLIER,[7] JEAN FRANÇOIS GONZALEZ,[7,8] OLIVIER HAINAUT,[7] CHRIS LIDMAN,[7] BRUNO LEIBUNDGUT,[2] KEN'ICHI NOMOTO,[5] TAKAYOSHI NAKAMURA,[5] JASON SPYROMILIO,[2] LUCA RIZZI,[3] MASSIMO TURATTO,[3] JEREMY WALSH,[2] TITUS J. GALAMA,[9] JAN VAN PARADIJS,[9,10,11] CHRYSSA KOUVELIOTOU,[12] PAUL M. VREESWIJK,[9] FILIPPO FRONTERA,[13] NICOLA MASETTI,[13] ELIANA PALAZZI,[13] AND ELENA PIAN[13]

Received 2000 June 21; accepted 2001 March 6

ABSTRACT

We present and discuss the photometric and spectroscopic evolution of the peculiar SN 1998bw, associated with GRB 980425, through an analysis of optical and near-IR data collected at ESO–La Silla. The spectroscopic data, spanning the period from day −9 to day +376 (relative to *B* maximum), have shown that this supernova (SN) was unprecedented, although somewhat similar to SN 1997ef. Maximum expansion velocities as high as 3×10^4 km s^{-1} to some extent mask its resemblance to other Type Ic SNe. At intermediate phases, between photospheric and fully nebular, the expansion velocities ($\sim 10^4$ km s^{-1}) remained exceptionally high compared to those of other recorded core-collapse SNe at a similar phase. The mild linear polarization detected at early epochs suggests the presence of asymmetry in the emitting material. The degree of asymmetry, however, cannot be decoded from these measurements alone. The He I 1.083 and 2.058 μm lines are identified, and He is suggested to lie in an outer region of the envelope. The temporal behavior of the fluxes and profiles of emission lines of Mg I] λ4571, [O I] $\lambda\lambda$6300, 6364, and a feature ascribed to Fe are traced to stimulate future modeling work. The uniqueness of SN 1998bw became less obvious once it entered the fully nebular phase (after 1 yr), when it was very similar to other Type Ib/c–IIb objects, such as the Type Ib SN 1996N and the Type IIb SN 1993J, even though SN 1998bw was 1.4 mag brighter than SN 1993J and 3 mag brighter than SN 1996N at a comparable phase. The late-phase optical photometry, which extends up to 403 days after *B* maximum, shows that the SN luminosity declined exponentially but substantially faster than the decay rate of ^{56}Co. The ultraviolet-optical-infrared bolometric light curve, constructed using all available optical data and the early *JHK* photometry presented in this work, shows a slight flattening starting on about day +300. Since no clear evidence of ejecta-wind interaction was found in the late-time spectroscopy (see also the work of Sollerman and coworkers), this may be due to the contribution of the positrons since most γ-rays escape thermalization at this phase. A contribution from the superposed H II region cannot, however, be excluded.

Subject headings: gamma rays: bursts — supernovae: general — supernovae: individual (SN 1998bw)

1. INTRODUCTION

SN 1998bw was discovered by Galama et al. (1998b) in the *BeppoSAX* Wide-Field Camera error box of GRB 980425 (Soffita et al. 1998; Pian et al. 1999) close to a spiral arm of the barred galaxy ESO 184-G82, by comparing two frames taken at the ESO New Technology Telescope (NTT) on April 28.4 and May 1.3 UT. Spectroscopic and photometric observations, both in the optical and in the near-IR, started at ESO–La Silla immediately after the discovery and showed that this object was profoundly different from all then known supernovae (SNe; Lidman et al. 1998). The peculiar spectrum led to diverse classifications. A few days after its detection, the object was classified as an SN Ib (Sadler et al. 1998) and later as a peculiar SN Ic (Patat & Piemonte 1998a; Filippenko 1998) owing to the complete absence of H lines, the weakness of the Si II λ6355 line, and no clear He I detection in the optical spectra.

Its peculiar spectroscopic appearance (Galama et al. 1998a; Iwamoto et al. 1998), its unusually high radio luminosity at early phases (Kulkarni et al. 1998), and, in particular, the probable association with GRB 980425 through positional and temporal coincidence (Galama et al. 1998a; Pian et al. 1999) placed SN 1998bw at the center of discussion concerning the nature of γ-ray bursts (GRBs; Wheeler 2001).

Independent photometric and spectroscopic data sets have been presented by several authors, whose results will be discussed and compared with those presented here

[1] Based on observations collected at ESO–La Silla.

[2] European Southern Observatory, Karl Schwarzschild Strasse 2, D-85748 Garching bei München, Germany; fpatat@eso.org.
[3] Osservatorio Astronomico di Padova, via Osservatorio 5, I-35122 Padova, Italy.
[4] Osservatorio Astronomico di Trieste, via G. B. Tiepolo 11, I-34131 Trieste, Italy.
[5] Research Centre for the Early Universe and Department of Astronomy, University of Tokyo, Bunkyo-ku, Tokyo 113-0033, Japan.
[6] Stockholm Observatory, S-133 36 Saltsjöbaden, Sweden.
[7] European Southern Observatory, Alonso de Cordova 3107, Casilla 19001 Santiago, Chile.
[8] Centre de Recherche Astronomique de Lyon, (CNRS-UMR 5574) Ecole Normale Supérieure 46 allée d'Italie, F-69364 Lyon Cedex 07, France.
[9] Astronomical Institute Anton Pannekoek CHEAF, Kruislaan 403, 1098 SJ Amsterdam, Netherlands.
[10] Department of Physics, University of Alabama in Huntsville, Huntsville, AL 35899.
[11] Deceased 1999 November 2.
[12] NASA Marshall Space Flight Center, SD-40, Huntsville, Alabama 35812.
[13] Istituto Tecnologie e Studio Radiazioni Extraterrestri, CNR, Bologna, Italy.

throughout the paper. Here we give only a brief account of the main results of these previous works.

The early light curve of SN 1998bw has shown that the object was unusually bright when compared to known SNe of Type Ib/c ($M_V \sim -19.2 + 5 \log h_{65}$; Galama et al. 1998a). The broadband photometric observations by McKenzie & Schaefer (1999) taken during the intermediate phases (47–171 days after maximum brightness) revealed that the object settled on an exponential decay similar to that observed in other Type Ic SNe. McKenzie & Schaefer first suggested that even in this case the light curve was powered by the radioactive decay of ^{56}Co with some leakage of γ-rays. Finally, the late-phase light curve was covered up to 500 days from the explosion by the observations of Sollerman et al. (2000). Their models achieved a fairly good reproduction of the data with the radioactive material well mixed in the ejecta and $M(^{56}\mathrm{Ni}) \sim 0.5\ M_\odot$.

The peculiar spectroscopic behavior of SN 1998bw around maximum light has been presented and discussed by Iwamoto et al. (1998), who identified the main spectral features as O I, Ca II, Si II, and Fe II. The estimated expansion velocities were exceptionally high ($\sim$30,000 km s^{-1}), and this caused a severe line blending. The evolution during the first months was unusually slow compared to known Type Ic SNe, with the nebular spectra still retaining many of the features present during the photospheric phase (Patat et al. 2000; Stathakis et al. 2000). The late onset of the fully nebular phase has been interpreted as an indication of a large ejected mass (Stathakis et al. 2000) since it was predicted by the early light-curve models (see below). During the intermediate phase, the emission lines were definitely broader than in known Type Ib/c supernovae, and the simultaneous presence of iron-peak and α-elements indicated unusual relative abundances or physical conditions in the SN ejecta (Patat & Piemonte 1998b; Patat et al. 2000). The late spectroscopy presented by Sollerman et al. (2000) showed that the tentative morphological classification of SN 1998bw as a Type Ic event was indeed appropriate. The main features have been identified as [O I], Ca II, Mg I, and Na I D, the latter possibly contaminated by He I λ5876.

Photometric and spectroscopic modeling of the early phases and the possible connection with GRB 980425 have been discussed by Galama et al. (1998a), Iwamoto et al. (1998), Höflich, Wheeler, & Wang (1999), Woosley, Eastman, & Schmidt (1999), and Pian et al. (1999).

The symmetric models of the early spectra and light curve by Iwamoto et al. (1998) and Woosley et al. (1999) reached a similar conclusion: SN 1998bw was generated by an extremely energetic explosion of a $\sim 10\ M_\odot$ C-O star, which ejected 0.5–0.7 $M_\odot$ of ^{56}Ni. This large amount of radioactive material, which is 1 order of magnitude larger than that estimated for known core-collapse SNe (Patat et al. 1994; Schmidt et al. 1994), is required to power the early light curve. In these models the explosion energy must be large to accelerate the ejected mass ($\sim 10\ M_\odot$) to the observed velocities and to make the light curve peak in only 19 days. Actually, in spherical symmetry, the light curve around maximum can be reproduced using different combinations of explosion energy and envelope mass. This degeneracy was resolved by Iwamoto et al. (1998) using velocity information and computing synthetic spectra for the various candidate models.

An alternative scenario was proposed by Höflich et al. (1999), who used less energetic asymmetric models and a suitable combination of viewing angle and degree of asymmetry. The required mass of ^{56}Ni is in this case 0.2 $M_\odot$. This low mass of radioactive material, however, seems too low to explain the late emission of the supernova (Sollerman et al. 2000).

In this paper we report on the results of an extensive observational campaign carried out at ESO–La Silla, which covered the evolution of SN 1998bw from the discovery until 417 days after the GRB detection. The paper is organized as follows: In § 2 we discuss the observations and reduction techniques for the optical and the near-IR. The evolution of SN 1998bw around maximum light is discussed in §§ 3, 4, and 5, which deal with low-resolution spectroscopy, polarimetry, and high-resolution spectroscopy, respectively. The He I detection in the near-IR spectra is presented in § 6, in which possible alternatives to the He I identification are also investigated. The description of SN 1998bw's metamorphosis ends in § 7, where we follow its evolution into the nebular phase. The late-phase light curves are presented and compared with those of other SNe in § 8. This section also presents the ultraviolet-optical-infrared (UVOIR) bolometric light curve, which is compared to the model of Iwamoto et al. (1998). Finally, § 9 summarizes our conclusions.

2. OBSERVATIONS AND DATA REDUCTION

2.1. *Optical Spectroscopy*

Spectroscopic observations were obtained from early to late phases using the ESO 1.52 m (Boller and Chivens spectrograph), ESO-Danish 1.54 m (DFOSC), ESO 3.6 m (EFOSC2), and ESO-NTT (EMMI) telescopes. Exposure times ranged from 10 minutes near maximum light to several hours at late phases. The journal of spectroscopic observations is shown in Table 1.

The spectra were reduced using IRAF packages.[14] For some of the spectra taken at the ESO-Danish telescope, it was not possible to remove the fringing in the red since suitable flat fields were not available. This gives rise to the high-frequency modulation of the spectra at wavelengths longer than 7500 Å.

Particular care was devoted to the extraction of the SN spectra to avoid contamination from the host galaxy background. Nevertheless, especially in the late-phase spectra, the contribution from an underlying H II region could not be completely eliminated, and thus unresolved narrow lines (Hα, Hβ, [O II], [O III]) appear in the reduced spectra. We emphasize that these features do not show a coherent time evolution but rather depend on seeing conditions and slit position. For this reason we conclude that they are not intrinsic to the SN. Finally, there is no evidence of continuum contamination from the parent galaxy.

Wavelength calibration was achieved by using arc spectra from He-Ne-Ar lamps, while the response curves were obtained via observations of spectrophotometric standard stars (Oke 1990; Hamuy et al. 1992). The accuracy of the absolute flux calibration was finally checked against the broadband photometry and, when necessary, adjusted accordingly.

On 1998 May 6, two high-resolution spectra of SN 1998bw, covering the region 3750–7650 Å, were obtained at the ESO-NTT using EMMI in the echelle mode, with a

[14] IRAF is distributed by the National Optical Astronomy Observatories, which are operated by the Association of Universities for Research in Astronomy, Inc., under contract to the National Science Foundation.

TABLE 1

JOURNAL OF SPECTROSCOPIC OBSERVATIONS

Date	JD (2,400,000+)	Phase[a] (days)	Range (Å)	Resolution FWHM[b] (Å)	Equipment	Standard Stars
1998 May 1.3	50,934.8	−9	5900–9200	10	NTT-EMMI	G138−31
1998 May 3.4	50,936.9	−7	3350–9000	10	Danish	LTT 7379
1998 May 4.3	50,937.8	−6	3400–10250	20	ESO 3.6 m	CD 32d9927
1998 May 4.4	50,937.9	−6	3400–7550	20	ESO 3.6 m–Pol.	HD 161056
1998 May 6.3	50,939.8	−4	3750–7650	1	NTT-ECH	...
1998 May 7.3	50,940.8	−3	3500–9000	10	Danish	LTT 7379
1998 May 8.3	50,941.8	−2	3350–10150	10	Danish	LTT 7379
1998 May 9.3	50,942.8	−1	3300–10150	10	Danish	LTT 7379
1998 May 11.2.....	50,944.7	+1	3450–10200	10	Danish	LTT 7379
1998 May 13.4.....	50,946.9	+3	3450–10200	10	Danish	LTT 7379
1998 May 14.4.....	50,947.9	+4	3350–8900	10	Danish	LTT 7379
1998 May 16.4.....	50,949.9	+6	3400–9000	10	Danish	LTT 7379
1998 May 18.3.....	50,951.8	+8	9500–25200	18	NTT-SofI	Hip 106725
1998 May 19.4.....	50,952.9	+9	3250–9000	10	Danish	EG 274
1998 May 20.3.....	50,953.8	+10	3400–7550	20	ESO 3.6 m–Pol.	HD 161056
1998 May 21.4.....	50,954.9	+11	3400–9000	10	Danish	LTT 6248
1998 May 22.4.....	50,955.9	+12	3400–9000	10	Danish	LTT 7379
1998 May 23.3.....	50,956.8	+13	3100–10200	15	ESO 1.52 m	Feige 110
1998 May 29.4.....	50,962.9	+19	3350–10250	20	ESO 3.6 m	LTT 7379
1998 Jun 1.3	50,965.8	+22	3400–9000	10	Danish	LTT 6248
1998 Jun 8.2	50,972.7	+29	4200–9000	10	Danish	LTT 6248
1998 Jun 12.3	50,976.8	+33	9500–25200	18	NTT-SofI	G2720
1998 Jun 24.2	50,988.7	+45	3400–9000	10	Danish	LTT 6248
1998 Jun 30.3	50,994.8	+51	9500–25200	18	NTT-SofI	BS 4620, BS 6823
1998 Jul 1.2	50,995.7	+52	3400–9000	10	Danish	LTT 7987
1998 Jul 13.2.....	51,007.7	+64	3400–9000	10	Danish	LTT 6248
1998 Jul 22.3.....	51,016.8	+73	3100–10100	15	ESO 1.52 m	Feige 110
1998 Aug 12.2	51,037.7	+94	3100–10100	15	ESO 1.52 m	Feige 110
1998 Sep 12.2.....	51,068.7	+125	3400–10200	20	ESO 3.6 m	Feige 110
1998 Nov 26.0	51,144.5	+201	3350–10200	20	ESO 3.6 m	LTT 1020
1999 Apr 12.4	51,280.9	+337	3350–10250	20	ESO 3.6 m	LTT 6248, LTT 7379
1999 May 21.2.....	51,319.7	+376	3350–10250	17	ESO 3.6 m	LTT 3864, Feige 110
1999 May 21.2.....	51,319.7	+376	4750–6750	7	ESO 3.6 m	LTT 3864, Feige 110

NOTES.—NTT-EMMI = ESO NTT + EMMI + TK2048 (red arm) + TH1024 (blue arm), NTT-ECH = NTT + EMMI echelle mode + TK2048, Danish = ESO Danish 1.54 + DFOSC + Loral/Lesser 2048, ESO 3.6 m = ESO 3.6 m + EFOSC2 + Loral/Lesser 2048, ESO 3.6 m–Pol. = ESO 3.6 m + EFOSC2 + Polarimeter + Loral/Lesser 2048, NTT-SofI = ESO NTT + SofI + Rockwell Hg:Cd:Te 1024, ESO 1.52 m = ESO 1.52 m + B&C + Ford 2048.

[a] Relative to *B* maximum (JD = 2,450,943.8).

[b] FWHM of night sky lines.

7″-long and 2.″0-wide slit (resolution 1 Å FWHM at 5900 Å, i.e., 50 km s^{-1}). Order definition and extraction, sky subtraction, and wavelength rebinning were achieved using the IRAF echelle reduction package. The orders were merged and the two exposures combined to a weighted mean to give the final spectrum, which was eventually flux calibrated by comparison with a medium-resolution spectrum of the SN taken the following day (see Table 1). A signal-to-noise ratio of about 15 in the region of the Na I D doublet was achieved.

2.2. *IR Photometry and Spectroscopy*

Near-IR photometry of SN 1998bw was obtained at three epochs with SofI at the ESO-NTT (see Table 2) through the *J*, *H*, and *K* passbands (Bessell & Brett 1988). In order to allow for a proper sky subtraction, the target was observed using the jittering technique. The reductions were performed in a standard way within IRAF, and the fluxes were estimated via plain aperture photometry, since at those early epochs the contribution from the host galaxy was

TABLE 2

IR PHOTOMETRY OF SN 1998bw

Date	JD (2,400,000+)	Phase[a] (days)	*J*	*H*	*K*	Seeing (arcsec)	Telescope
1998 May 18.3.....	50,951.8	+8	13.40 ± 0.04	13.35 ± 0.04	13.15 ± 0.04	0.7	NTT + SofI
1998 Jun 12.3	50,976.8	+33	14.41 ± 0.04	14.25 ± 0.04	14.20 ± 0.04	1.2	NTT + SofI
1998 Jun 30.3	50,994.8	+51	15.11 ± 0.04	14.98 ± 0.04	14.89 ± 0.04	0.9	NTT + SofI

[a] Relative to *B* maximum (JD = 2,450,943.8). This occurred 14.4 days after GRB 980425.

TABLE 3

LATE-PHASE PHOTOMETRIC OBSERVATIONS OF SN 1998bw

Date	JD (2,400,000+)	Phase[a] (days)	U	B	V	R	I	Seeing (arcsec)	Telescope
1999 Mar 16.1.....	51,253.6	+310	...	20.69 ± 0.07	20.52 ± 0.07	...	...	1.3	Dutch 0.9 m
1999 Mar 17.1.....	51,254.6	+311	...	20.71 ± 0.07	20.50 ± 0.07	19.74 ± 0.05	...	1.3	Dutch 0.9 m
1999 Apr 8.1.....	51,276.6	+333	...	21.10 ± 0.15	20.69 ± 0.15	20.09 ± 0.15	...	1.1	ESO 3.6 m
1999 Apr 12.2	51,280.7	+337	21.13 ± 0.20	...	...	...	20.03 ± 0.15	1.1	ESO 3.6 m
1999 May 21.2.....	51,319.7	+376	...	21.59 ± 0.20	21.43 ± 0.20	20.83 ± 0.20	20.61 ± 0.20	1.2	ESO 3.6 m
1999 Jun 17.3.....	51,346.8	+403	21.69 ± 0.20	21.91 ± 0.20	21.70 ± 0.20	20.87 ± 0.20	20.76 ± 0.20	1.0	ESO 3.6 m

NOTES.—Dutch 0.9 m = 0.92 m ESO-Dutch + CCD TK512, ESO 3.6 m = ESO 3.6 m + EFOSC2 + Loral/Lesser 2048.

[a] Relative to B maximum (JD = 2,450,943.8). This occurred 14.4 days after GRB 980425.

negligible. The photometric errors were estimated including the nightly zero-point variations, the aperture correction, and the photon shot noise.

Near-IR spectra of SN 1998bw were taken at the same epochs and with the same instrument used for the IR photometry. To cover the entire near-IR region, two grisms were used: one for the range 0.95–1.64 μm and one for the range 1.53–2.52 μm. The observations were made with the 1.″0 slit. The resulting resolving power, measured from the comparison xenon spectrum, was $\lambda/\Delta\lambda \sim 600$ for both grisms.

As is standard procedure for IR spectroscopy, the SN was observed at two positions along the slit, and the telescope was nodded between these two positions once every few minutes. The highly variable night sky is then accurately removed by combining all spectra in the appropriate way. Atmospheric features have been removed by dividing the extracted spectra by the spectra of nearby bright stars that were observed soon after the SN: HD 135591 (May 18; Perryman et al. 1997), Hipparcos 106725 (June 6; Perryman et al. 1997), and BS 4620 and BS 6823 (June 30; McGregor 1995). The stellar spectra often contain weak absorption lines from hydrogen (Paschen and Brackett series) and helium, which where removed before division. Wavelength calibration was achieved using comparison emission-line spectra of xenon gas lamps and is accurate to 1–2 Å. The spectra obtained with the two different grisms were then combined into a single spectrum.

Relative flux calibration was achieved by multiplying the spectrum by a blackbody curve with a temperature appropriate for the star used to remove the atmospheric features (HD 135591, $T = 30{,}000$ K; Hipparcos 106725, $T = 5800$ K; BS 4620, $T = 13{,}000$ K, and BS 6823, $T = 25{,}000$ K). Absolute flux calibration was performed by comparison to the broadband IR photometry at the same epochs.

2.3. *Polarimetry*

Spectropolarimetry of SN 1998bw was performed at two epochs (1998 May 4 and May 29) using the ESO 3.6 m telescope equipped with EFOSC2 in polarimetric mode (Patat 1999). A Wollaston prism was used with a focal plane mask to isolate the ordinary and extraordinary ray spectra of object and two sky positions; the separation of the two spectra is 20″. A half-wave plate was used to obtain spectra at four different position angles of 0.°0, 22.°5, 45.°0, and 67.°5. The B300 grism was used, giving a resolution of 10 Å over the wavelength range 3400–7550 Å. Table 1 provides a journal of the observations. The air mass was large at the time of the observations, and the spectral region at $\lambda < 4000$ Å is severely affected by differential atmospheric refraction. The *Hubble Space Telescope* (*HST*) polarized standard star HD 161056 (Turnshek et al. 1990) was observed on each night to check the polarization and position angle calibration.

The data were bias subtracted, and the ordinary and extraordinary ray spectra of SN 1998bw were extracted with the local sky subtracted. Statistical errors were assigned to each extracted spectrum using the known properties of the detector (CCD ESO No. 40; Patat 1999). The data were then combined, following the procedure outlined by Tinbergen & Rutten (1992), and the total spectrum, linear polarization, and position angle were computed using dedicated programs running in the ESO MIDAS package (see Walsh 1992). The polarization was binned into equal wavelength width bins to provide polarization errors per bin below 0.1% over the wavelength range 4000–7000 Å. For observations of HD 161056, the measured polarization in the V band was 4.3% at position angle (P.A.) 76°, in satisfactory agreement with the standard value of 4.04% at P.A. = 67°, given that Turnshek et al. (1990) suggest that it may be variable in polarization.

2.4. *Optical Photometry*

Late-time optical broadband photometry of SN 1998bw in the Johnson-Cousins *UBVRI* photometric system (Bessell 1990) was obtained in the phase range 310–403 days from B maximum. Table 3 shows the journal of the photometric observations, which were performed with the ESO-Dutch 0.9 m telescope, equipped with a TEK coated 512 × 512 pixel CCD (scale 0.″44 pixel^{-1}), and with the ESO 3.6 m telescope, equipped with EFOSC2 (Loral/Lesser 2048 × 2048 pixel CCD, scale 0.″16 pixel^{-1}). The SN is located on a spiral arm and superimposed on an H II region, which is clearly visible in Figure 1. At late phases the background contribution is significant, and the SN magnitude cannot be measured using plain aperture photometry. Therefore, after the standard bias and flat-field corrections, magnitude measurements were obtained by means of the point-spread function fitting technique implemented in SNOoPY (Patat 1996), a package specifically designed for SN photometry within the IRAF environment.

Color terms for the two instruments have been computed using observations of standard fields (Landolt 1992). The SN magnitudes have been calibrated by means of relative photometry with respect to the local sequence defined by P. M. Vreeswijk et al. (2001, in preparation; stars 1–10). The results of the late photometry here presented are in good agreement with those recently published by Sollerman et al. (2000).

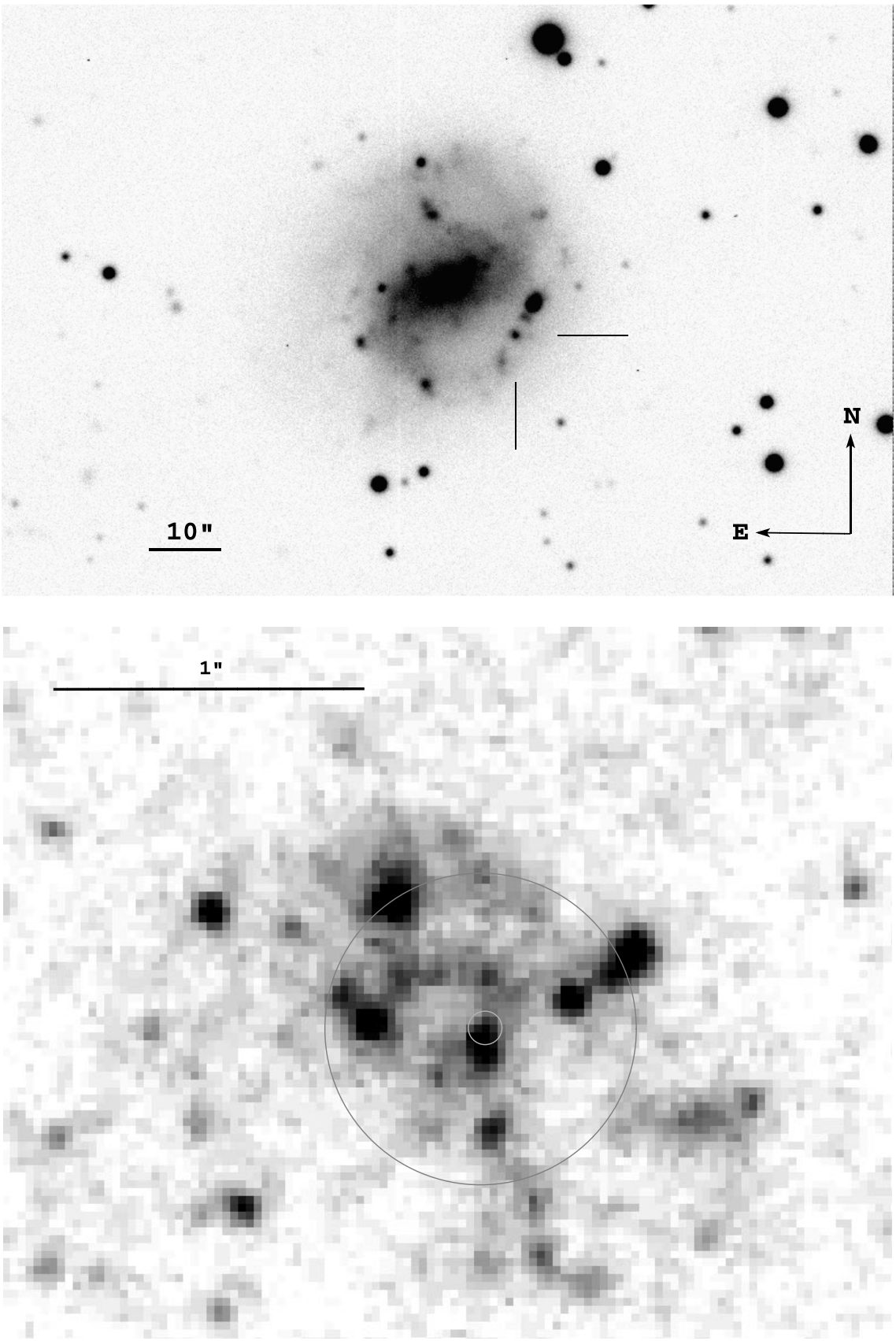

FIG. 1.—*Upper panel*: SN 1998bw in ESO 184-G82. The frame was obtained on 1999 June 17 (403 days after *B* maximum light) in the *R* band (5 minutes) with the ESO 3.6 m + EFOSC2. *Lower panel*: *HST* + STIS image of SN 1998bw environment at about 764 days after *B* maximum light (Fynbo et al. 2000). The SN location is marked by a small circle, and the big circle centered on the SN position has a diameter of 1″.

3. SPECTROSCOPIC EVOLUTION AROUND MAXIMUM LIGHT

The spectral behavior of SN 1998bw from day +7 to day +94 has already been discussed by Stathakis et al. (2000). The larger wavelength range and improved phase coverage of the data we are presenting here allow us to analyze the early phases in more detail and to push the discussion further into the late evolutionary stages. For a discussion of an independent late-phase data set, see Sollerman et al. (2000).

The spectroscopic evolution of SN 1998bw around maximum light is presented in Figure 2. Wavelengths are corrected to the parent galaxy rest frame, adopting $v_{gal} = 2532$ km s^{-1}, as measured from the narrow Hα emission line (see § 5). Phases are from *B* maximum, whose epoch (1998 May 10 UT) was estimated from the photometric data presented by Galama et al. (1998a). It occurred 14.4 days after the detection of GRB 980425. We adopt these conventions throughout the paper.

The general appearance of the spectrum at maximum light is quite unique among SNe, even though it is somewhat reminiscent of SN 1997ef (Filippenko 1997b; P. M. Garnavich et al. 2001, in preparation), which has been modeled as a massive SN Ic event (Iwamoto et al. 2000; Mazzali, Iwamoto, & Nomoto 2000). This appears clearly in Figure 3, where the spectrum of SN 1998bw is compared to those of other Type I SNe.

Another striking feature is the redward shift with time of most of the spectral features, both in absorption and in emission. At early phases the apparent broad emission-like features do not result from discrete emission lines but occur where absorption-line optical depths are low, and photons redshifting in the expanding ejecta, as a result of absorption and scattering processes, have a higher probability of escaping (see, for example, Mazzali 2000; Pinto & Eastman 2000). Thus, while the shift of the absorption lines can be understood as the effect of the inward recession of the photosphere, that of the emission features requires a clearer knowledge of which lines are contributing to absorption and how this changes with velocity (i.e., comoving radius). The effect is also shown in Figure 4, where the evolution of the Si II λ6355 region has been plotted.

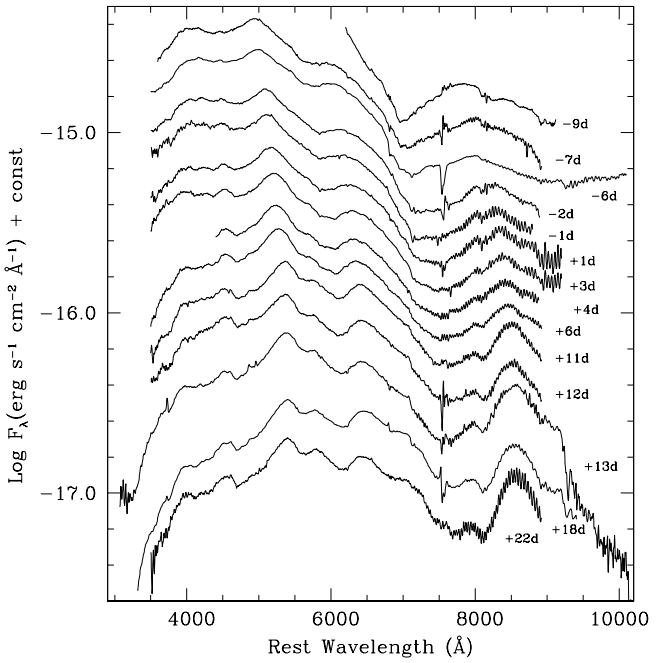

FIG. 2.—Spectroscopic evolution of SN 1998bw from day −9 to day + 22. For presentation the spectra have been vertically shifted by arbitrary amounts: -7^d (−0.40, log F_λ), -6^d (−0.60), -2^d (−0.95), -1^d (−1.10), $+1^d$ (−1.30), $+3^d$ (−1.45), $+4^d$ (−1.60), $+6^d$ (−1.70), $+11^d$ (−1.75), $+12^d$ (−1.90), $+13^d$ (−2.10), $+19^d$ (−2.30), and $+22^d$ (−2.45). Spectra are in the host galaxy rest frame ($v_{gal} = 2532$ km s^{-1}; see § 5).

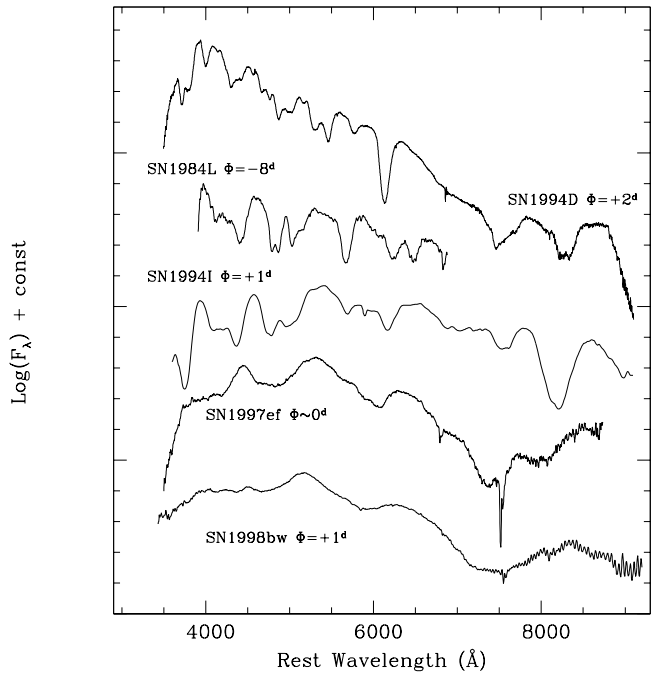

FIG. 3.—Comparison between SN 1998bw and other SNe at maximum light. Data are from Patat et al. (1996; 1994D), Harkness et al. (1987; 1984L), ESO-KP database (1994I), and Garnavich et al. (2001, in preparation; 1997ef). All spectra have been corrected to the parent galaxy rest frame adopting the following recession velocities: SN 1998bw, 2532 km s^{-1} (see § 5); SN 1997ef, 3504 km s^{-1}; SN 1994I, 463 km s^{-1}; SN 1994D, 448 km s^{-1}; SN 1984L, 1934 km s^{-1} (de Vaucouleurs et al. 1991).

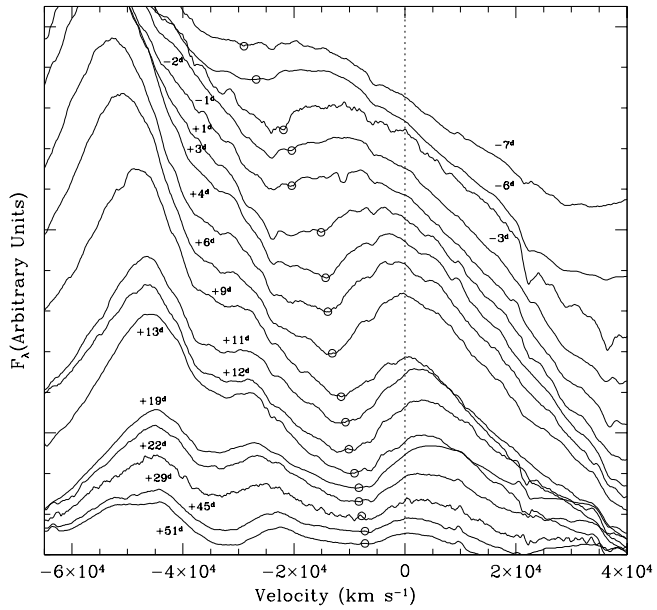

FIG. 4.—Evolution of the Si II λ6355 region. The empty circles mark the value that has been assumed to represent the photospheric velocity.

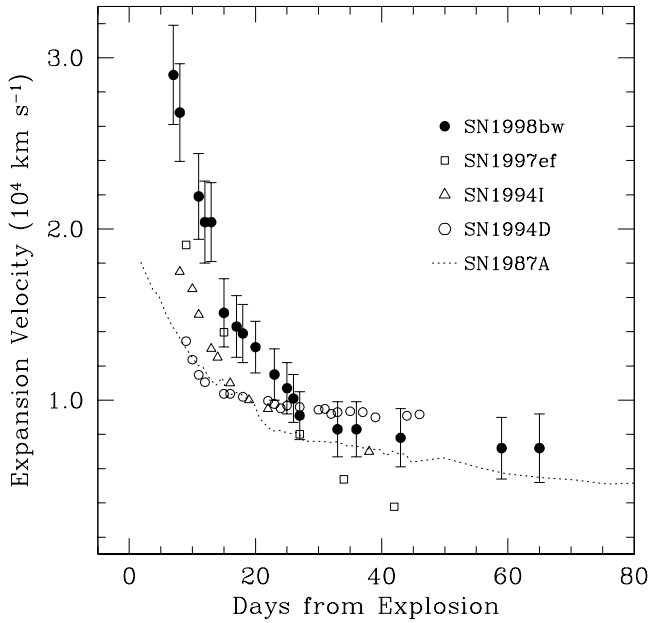

FIG. 5.—Si II λ6355 expansion velocity evolution of SN 1998bw compared with SN 1994D (Patat et al. 1996), SN 1994I (Millard et al. 1999), and SN 1997ef (Garnavich et al. 2001, in preparation). For comparison the photospheric expansion velocities deduced from the Hα absorption minima of SN 1987A are also plotted (Phillips et al. 1988).

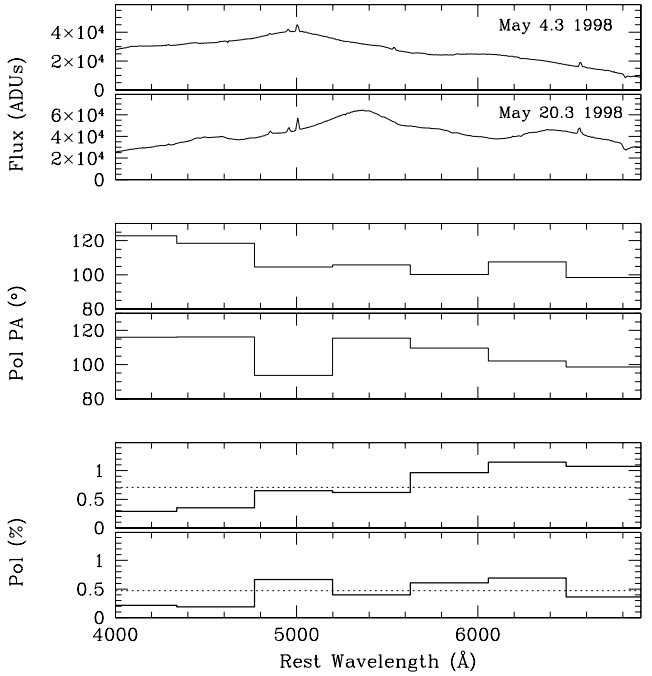

FIG. 6.—Raw spectrum (ADU), position angle (degrees) and linear polarization degree (percent) are shown from the EFOSC2 spectropolarimetry observations at day −7 (*upper panel*) and day +10 (*lower panel*). Wavelengths are corrected to the host galaxy rest frame (v_{gal} = 2532 km s^{-1}; see § 5). The linear polarization and position angle data have been binned into 200 channel increments to increase the signal-to-noise ratio.

In these early phases when the velocity is high, line blending is particularly severe. The modeling presented by Iwamoto et al. (1998) suggests that the main features are due to lines of Si II, O I, Ca II, and Fe II. The time evolution of the expansion velocity at the photosphere, as deduced from the minimum of the absorption trough of the Si II λ6355 line, is shown in Figure 5. For comparison, the corresponding values measured for the Type Ia SN 1994D, the Type Ic SN 1994I[15], and the peculiar Type Ic SN 1997ef are also plotted. SN 1998bw shows a sudden break in the expansion velocity decline rate around day 15 and another at day 27. While changes in the slope are to be expected as a result of changes in optical depth at line center, the reasons for sudden changes are not clear. There is no doubt that the velocity decline rate changes significantly; what is less clear, in view of measurement uncertainties, is how suddenly they occurred.

The velocity deduced from the Si II λ6355 line is about 30,000 km s^{-1} at day −7 and decreases to about 8000 km s^{-1} at day +22. These values are exceptionally high, for any SN, as can be seen in Figure 5. SN 1994I shows a trend that is very similar to that of SN 1998bw, although the velocities are systematically lower, while SN 1997ef deviates significantly after day 25 (Fig. 5). Phases for SN 1997ef are uncertain because maximum light was not recorded.

4. POLARIMETRY

In order to investigate any possible asphericity in the explosion of SN 1998bw, spectropolarimetry measurements were performed at two epochs (day −7 and day +10; see Table 1). The polarization averaged over the range 4000–7000 Å was 0.7% and 0.5% at the two epochs, respectively. Figure 6 shows the total spectrum (raw, not flux calibrated), the polarization binned into 200 channel bins, and the position angle of the polarization vector projected on the sky at both epochs. The formal errors per bin are about 0.04%, but the error on the polarization binned over the optical range is 0.1% given that the measurements were not of high photometric quality and the discrepancy on the measurement of the polarized standard. It appears that the polarization spectrum at day −7 has a significant increase to the red that is not in evidence at the later epoch. In terms of the integrated polarization over the 4000–7000 Å range, there may be a marginal change in the polarization between the two epochs, but no great significance is attached to this result.

The interstellar polarization in the direction of the host galaxy can be estimated by the measurement of stellar polarization along a nearby sight line. Kay et al. (1998) measured the linear polarization of HD 184100 at 0.75% in P.A. 176°.5. Correcting the linear polarization results by this value of interstellar polarization results in 0.6% at P.A. 80° and 0.4% at 67° at days −7 and +10, respectively. The polarization value is not very different from the value of 0.53% measured by Kay et al. (1998) at day ∼42 and is most probably intrinsic to the SN, although a dusty medium in the SN parent galaxy cannot be ruled out. However, the position angles differ from the Kay et al. value of 49°, although the errors on these earlier determinations are larger (at least 5°). Despite its association with a γ-ray burst, these polarization values are similar to those reported for other core-collapse SNe (Wang et al. 1996).

The small degree of polarization at optical wavelengths can be explained in terms of a moderate departure from sphericity (axial ratio less than 2:1; Höflich 1995; Höflich et al. 1999) either in the photosphere or in the outer scattering envelope when the line of sight is not coincident with

[15] The data for SN 1994I are from the ESO Key Project on Supernovae database (hereafter ESO-KP; Turatto et al. 1990).

an axis of symmetry. Unfortunately, it is not possible from polarization measurements alone to decode both the shape of the object and the viewing angle, and therefore the small polarization values reported here could indicate large departures from sphericity but viewed close to an axis of symmetry or small departures viewed well away from the symmetry axis. Net polarization could also result from a spherical envelope in which, as a result of large-scale clumping, one hemisphere had a surface brightness different from that of the other hemisphere. Delayed light echoes could also be responsible for the observed polarization, provided that the time delay is comparable to the timescale of the SN luminosity variation.

We note that no polarization, either circular or linear, was detected in the radio, and this has been interpreted as the signature of a spherically symmetric blast wave (Kulkarni et al. 1998). This apparent discrepancy might suggest that the radio and the optical radiation were generated in regions of different geometry.

5. HIGH-RESOLUTION SPECTROSCOPY

To search for possible narrow emission lines produced in the circumstellar environment of the progenitor and for interstellar absorption features, we obtained high-resolution spectra of SN 1998bw around maximum brightness. With the exception of a narrow Hα emission line centered at 2532 km s^{-1} and probably arising from the underlying H II region (see also § 2.1 and Tinney, Stathakis, & Cannon 1998), neither the usual Na I D absorption lines, which would signal intervening interstellar dust, nor narrow emission lines were detected. However, the signal-to-noise ratio we achieved (SNR $\sim$ 20 at Hα and $\sim$15 at Na I D) is insufficient to exclude the presence of lines, both in emission and absorption, with EW $\leq$ 0.2 Å. Using the relation recently calibrated by S. Benetti, E. Cappellano, P. Mazzali, F. Patat, & M. Turatto (2001, in preparation) and assuming that the total EW of the Na I D doublet is EW $\leq$ 0.4 Å, one can estimate an upper limit for the extinction, $A_V \leq 0.2$. There are two values of A_V available in the literature, i.e., $A_V = 0.05$ (Burstein & Heiles 1982) and $A_V = 0.2$ (Schlegel, Finkbeiner, & Davis 1998). Both estimates are compatible with our upper limit, but we will assume $A_V = 0.2$ throughout this paper due to its more recent determination from *COBE*/DIRBE maps and the *IRAS* Infrared Sky Survey Atlas.

6. INFRARED SPECTRA: HELIUM AND OTHER ELEMENTS

The IR spectra are plotted in Figure 7. The most prominent feature is the broad emission at 1.08 μm, which has an associated P Cygni structure with a hint of more than one component in absorption. The main component of the emission and the absorption minimum at day +8 strongly suggest that this feature is due to He I 1.083 μm with a velocity of 18,300 ± 700 km s^{-1}. There is nevertheless the possibility that transitions from other ions are affecting this profile. The absorption does not seem to shift redward with time as shown in the upper panel of Figure 8. This is to be expected if the helium were confined to an outer higher velocity layer either optically thick or thin but restricted to a narrow velocity range. A more extended layer that had become optically thin on or before the date of the first IR spectrum could also in principle give rise to this constancy of velocity. The first interpretation is reinforced by the fact that at the same phase (i.e., 22.4 days after the explosion),

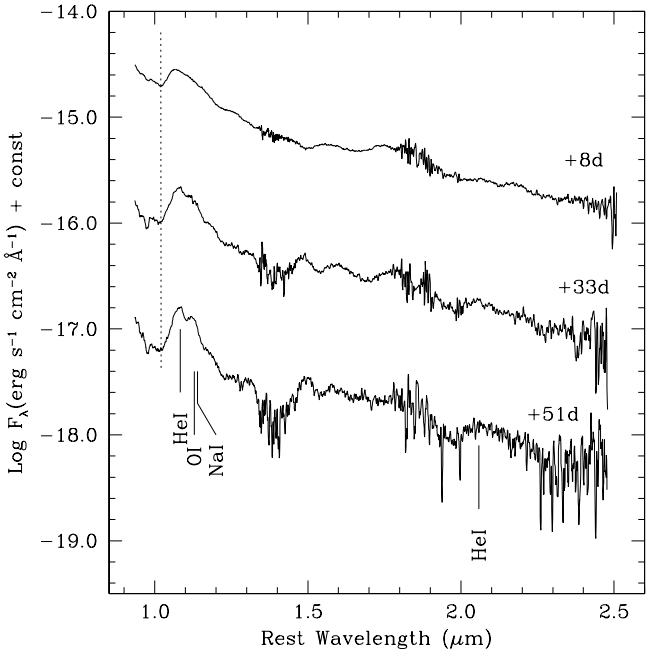

FIG. 7.—IR spectroscopic evolution of SN 1998bw from +8 to day +51. For presentation the last two spectra have been vertically shifted by an arbitrary amount: $+33^d$ (−0.80, log F_λ), $+51^d$ (−1.70). The vertical dotted line is placed at the wavelength of the absorption trough's minimum of He I 1.083 μm. The increased noise level in the wavelength ranges 1.35–1.45 and 1.8–1.9 μm is due to high atmospheric absorption. Spectra are in the host galaxy rest frame.

Si II λ6355 had a much smaller velocity (12,000 km s^{-1}), which may more closely indicate the photospheric velocity, at least up to day +22 (see Fig. 5). Since the color temperature of the envelope at those phases is not sufficiently high to radiatively or collisionally excite the required levels

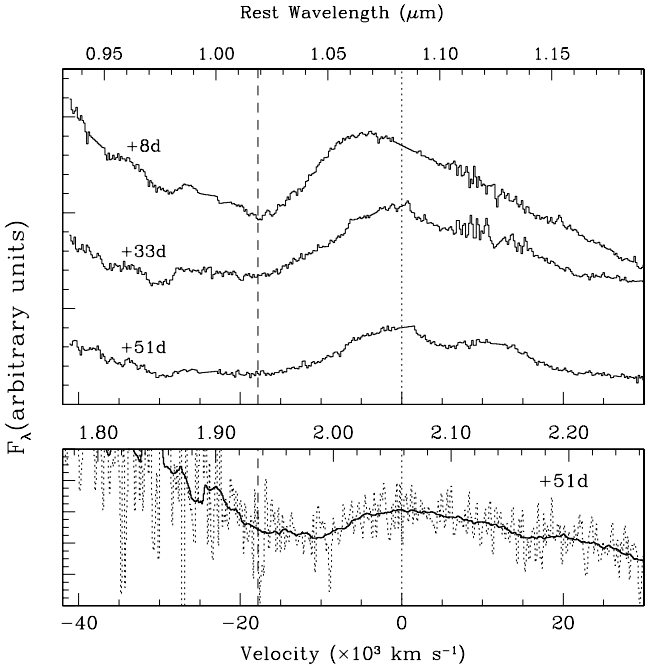

FIG. 8.—*Upper panel*: IR spectroscopic evolution of SN 1998bw from day +8 to day +51 in the region of He I 1.083 μm. The vertical dashed line marks the expansion velocity measured for He I 1.083 μm on day +8. *Lower panel*: Region of He I 2.058 μm at day +51. The solid line is a smoothed version of the spectrum. A 350 Å–wide boxcar filter was used.

of He I, one may conclude that excitation is caused by nonthermal electrons produced by γ-rays coming from the radioactive decay of ^{56}Co. This was predicted by Chugai (1987) for SN 1987A and shown to be effective by Graham (1988), Lucy (1991), and Mazzali & Lucy (1998) in various SNe, after Harkness et al. (1987) had identified He I lines by postulating large departures from LTE to explain the abnormal strengths.

He I has another transition (singlet series) in the near-IR, namely, at 2.058 μm ($2s^1S$–$2p^1P^0$). Careful inspection shows that in all three spectra a weak broad P Cygni feature is present at this wavelength (see Fig. 7). While this confirms the presence of He I in the spectra, because this spectral region is affected by strong telluric absorption, any line strength measurements should be treated with some caution. In the lower panel of Figure 8 the region centered on 2.058 μm is plotted for day +51, i.e., when this feature appears to be more pronounced. Even though the signal-to-noise ratio is poor, a P Cygni profile is visible and from the minimum of the absorption through an expansion velocity of 13,000 $\pm$ 2000 km s^{-1} is deduced, while the measured intensity ratio He I 1.083/He I 2.058 is about 30.

Since these He I lines show P Cygni profiles associated with strong continuum radiation, it is instructive to follow the qualitative results obtained by an elementary SN model in the Sobolev approximation (see, for example, Jeffery & Branch 1990). In that framework, the absolute emission line intensity not only depends on the line optical depth but also is proportional to the photospheric continuum intensity at the line wavelength. Thus, it is not surprising that the emission component of He I 1.083 μm is much greater than that of He I 2.058 μm. There is in fact roughly a factor 10 difference in the continuum flux at the two wavelengths, and therefore the measured intensity ratio translates into an equivalent width ratio EW(He I 1.083)/EW(He I 2.058) $\sim$ 3. The theoretical work by Lucy (1991) on the nonthermal excitation of helium in Type Ib SNe predicts a ratio close to 1 for these two He I features, whereas the ratio between the A-values is 5.2 (Martin 1987).

An additional complicating aspect to consider is that the He I 1.083 μm line originates from the metastable triplet ground state, which can give rise to resonance scattering not expected for the He I 2.058 μm line, whose lower level is metastable but whose upper level can be depopulated by an allowed transition to the singlet ground state. Moreover, the intensities of the two lines depend also on the fraction ϵ of collisional to total depopulations of the upper level of the transition. Hence, if one takes also into account that the optical depths of the two lines can be different, it is not surprising that the observed line ratio deviates from the expectations based on Einstein coefficients alone.

We note that the IR spectra of SN 1987A have shown a strong He I 1.083 μm line starting at day 110 (Meikle et al. 1989), from which an expansion velocity of 5000 km s^{-1} was deduced. The He I 2.058 μm line was also detected with an expansion velocity of 1500 km s^{-1}. Meikle et al. (1989) suggested that this is probably due to the fact that He I 2.058 μm was optically thin. For SN 1987A, the ratio He I 1.083/He I 2.058 in the phase range 110–349 days ranged from 23 to 50. In particular, on day 112 it was about 35; once one has taken into account the different continuum levels at the two wavelengths, this turns into an equivalent width ratio of about 6.

Very few other SNe have been observed in the 2 μm region. The Type II SN 1995ad and Type Ic SN 1997B have both shown a strong He I 1.083 μm feature without any evidence of the He I 2.058 μm line (Clocchiatti et al. 2001). He I 1.083 μm was identified also in the near-IR spectra of the Type IIn SN 1998S (Gerardy et al. 2000), and in that case, even though very faint, the He I 2.058 μm line was detected at 95 days after V maximum.

One possible difficulty with the identification of the 1.083 μm feature as He I comes from the apparent absence of the He I lines in the optical spectra at comparable phases. In Figure 9 we plot the optical spectra at days +6, +29, and +52, i.e., as close in time as possible to the IR spectra. At all three epochs, the spectrum is predominantly an absorption spectrum. Some of the strongest features tentatively identified using spectral synthesis are marked (*top*). We also marked the expected position of the He I absorption lines if they all had a blueshift of 18,300 km s^{-1} (*bottom*). The strongest optical line of He I should be λ5876, but this is blended with Na I D. He I λ5876 is clearly not present as a distinct individual feature at 18,300 km s^{-1}. There is no unambiguous sign of any other possible He I optical lines. This does not necessarily contradict the identification of the 1.083 μm feature as He I, because the optical lines can be suppressed relative to the IR ones if nonthermal excitation is at work (Mazzali & Lucy 1998). The large expansion velocity of SN 1998bw might also dictate greater blending effects in the optical region where the number of lines per unit wavelength is much larger than in the IR.

The optical He I lines are at least weaker than in the Type Ic SN 1994I. This SN also showed the He I 1.083 μm line (Filippenko et al. 1995) and possibly traces of He I contamination in the optical (Clocchiatti et al. 1996). Millard et al. (1999) have modeled SN 1994I's spectra and could fit the feature near 1.08 μm using a blend of C I 1.0695 μm and He I 1.083 μm, the latter being detached at 18,000 km s^{-1}. This

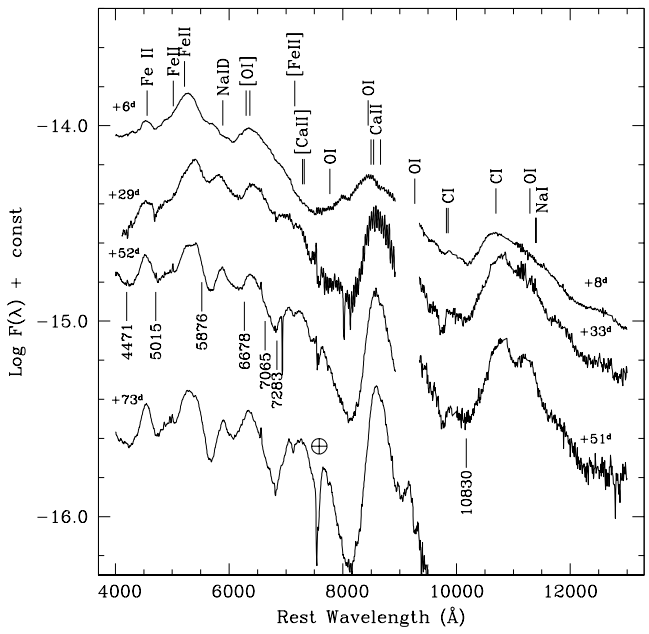

FIG. 9.—Optical and IR spectra of SN 1998bw at comparable phases. Line identifications from spectral modeling are plotted for the most prominent emission features (*top*) and for the He I lines (*bottom*). The He marks are placed at the expected absorption positions for an expansion velocity of 18,300 km s^{-1}.

velocity is similar to what is seen in SN 1998bw. However, they were able to obtain an alternative fit using only Si I lines. Another possibility is that the feature at 1.08 μm is due to Mg II 1.091 μm, as suggested by Mazzali & Lucy (1998) for the Type Ia SN 1994D.

Determining the amount of He in the ejecta is very important for constraining the nature of the progenitor and its evolutionary stage at the time of the explosion. Detailed spectral modeling, including nonthermal effects, is necessary for this purpose. Inclusion of helium in the exploding progenitor object may even affect our quantitative conclusions concerning the ejected mass, mass of radioactive material, kinetic energy, and mixing of the ejecta.

As the SN ages, the 1.083 μm emission feature develops a second, redder component (see Fig. 7). Possible identifications are O I 1.129 μm and Na I 1.138, 1.140 μm. The latter seems to be possible since its lower level is the upper level of the Na I D line transition, which would be well populated by resonance scattering. The Na I identification implies a velocity close to that of Si II λ6355 at the same phase and consistent with the Na I D line absorption. The presence of O I λ7771 in the optical is only a weak argument in favor of the O I 1.129 μm identification, since this latter line originates from a higher level.

7. ENTERING THE NEBULAR PHASE

The spectral evolution of SN 1998bw toward and during the nebular phase is presented in Figure 10, which shows all our spectra taken between day +29 and day +376. The transition from an absorption to an emission spectrum is slow and subtle and is marked by a decrease in the continuum.

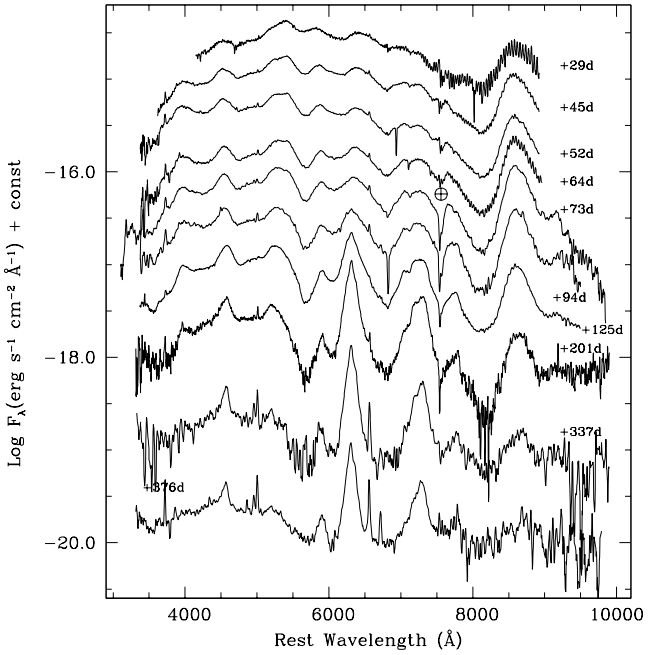

FIG. 10.—Spectroscopic evolution of SN 1998bw from day +29 to day +376. The phases have been computed from *B* maximum light (1998 May 10). For presentation the spectra have been vertically shifted by arbitrary amounts: +45^d (−0.20), +52^d (−0.55), +64^d (−0.95), +73^d (−1.20), +94^d (−1.50), +125^d (−1.70), +201^d (−1.90), +337^d (−2.00), and +376^d (−2.70). Narrow emission lines visible in the late-time spectra originate in the parent galaxy. Spectra are in the host galaxy rest frame.

While the evolution of SN 1998bw in the range 5500–9000 Å is similar to that of SN Ic events such as SN 1987M (Filippenko, Porter, & Sargent 1990), the expansion velocities are larger, and the region between 4000 and 5500 Å is dominated (at least until about day +200) by a wide bump to which Fe II transitions probably contribute significantly. The spectroscopic differences appear clearly in Figure 11, where SN 1998bw is compared to the Type Ia SN 1992A, the Type Ib SN 1996N, and the Type Ic SN 1996aq. From Figure 11 the late nebular spectrum of SN 1998bw appears to mostly resemble a Type Ic SN, in this case SN 1996aq. Mg I] λ4571 and [O I] λ6300 are present in both cases but not in the Type Ia SN 1992A. SNe Ia in general show strong [Fe II] and [Fe III] emission features not apparent in the same form in the two Type Ic SNe. In fact, the strongest spectral resemblance of SN 1998bw at nebular phases is to the peculiar SN 1985F and the Type Ic SN 1987M (Filippenko et al. 1990). Qualitatively, the appearance of Mg I and O I is consistent with what is expected from the nucleosynthesis model of Iwamoto et al. (1998) and their absence in models of Type Ia proposed by Nomoto et al. (1997).

All these facts support the general idea that SN 1998bw is related to SNe Ib/c. It might be regarded as an extreme case among these objects, having large kinetic energy, ejecta mass, and ejected mass of synthesized ^{56}Ni, while SN 1997ef could represent a less extreme case closer in properties to the known SNe Ic (see also Iwamoto et al. 2000; Mazzali et al. 2000; Stathakis et al. 2000; Branch 2001).

At late epochs the most prominent spectral feature is the [O I] $\lambda\lambda$6300, 6364 doublet. Figure 12 (*upper and middle panels*) reveals that this line has a complex profile, showing an apparently blended emission component blueshifted by approximately 2300 km s^{-1} with respect to the λ6300 doublet component. It is present at 201 and 376 days, and a similar feature appears to be present in the spectra of SN

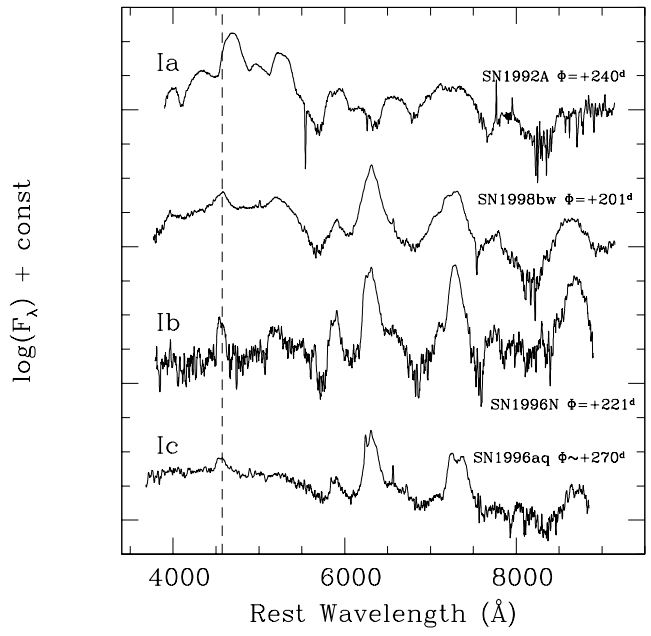

FIG. 11.—Comparison between SNe 1992A (Ia; ESO-KP database), 1998bw, 1996N (Ib; Sollerman et al. 1998), and 1996aq (Ic; ESO-KP database, unpublished) at late phases. The vertical dashed line is placed at the rest-frame wavelength of Mg I] λ4571.

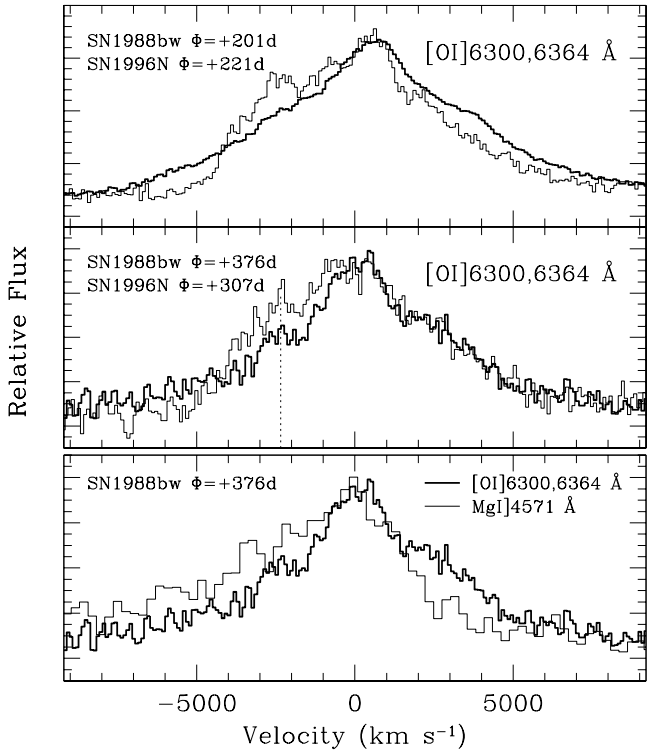

FIG. 12.—*Upper and middle panels*: The [O I] λλ6300, 6364 line profile at two different epochs for SN 1998bw (*thick line*) and SN 1996N (*thin line*; Sollerman et al. 1998). The vertical dotted line is placed at the position of the unidentified feature (see text). Velocities are computed from the λ6300 doublet component. *Lower panel*: Comparison between the profiles of [O I] λλ6300, 6364 (*thick line*) and MG I] λ4571 (*thin line*) for SN 1998bw at +376 days.

1996N at comparable phases. This therefore points to a common origin in the form of an as yet unidentified line (centered at ~6250 Å) or a similar structure (a clump?) in the line-emitting region.

The [O I] λ6300 line profiles are sharply peaked in the nebular phase, as are those of Mg I] λ4571, albeit a little less clearly. Uniform emission throughout the envelope should produce a parabolic profile, and therefore we can conclude that stronger emission is occurring at lower velocities in regions closer to the center (see also Maeda et al. 2000). A similar effect is apparent in other SNe, such as the Type Ic SN 1987M and peculiar SN 1985F (Filippenko et al. 1990), where it is also evident in emission lines of other ionic species.

Since Mg I] λ4571 seems to be the only single line in the spectrum with a sufficient signal-to-noise ratio, it is of some interest to study its behavior with time (see Fig. 13, *right panel*). At early stages prior to 100 days, the apparent emission feature must be dominated by some as yet unidentified feature because the peak is displaced blueward by 3500 km s^{-1} and gradually reaches the rest wavelength of Mg I] λ4571 at day 125. From this phase onward there is an excess in the blue wing causing an asymmetry, which becomes more marked as time passes by (see also Fig. 10). One explanation for this blue excess after day 201 is that it is the remnant of the unknown feature that dominated at early phases. It cannot be caused by the presence of Mg I] λ4562, which only reaches strengths comparable to that of Mg I] λ4571 at densities lower than a few 10^4 cm^{-3}, and in any case the separation is too small. A more interesting and plausible explanation for this blue component of Mg I] λ4571 is that it is the counterpart of the blue component of [O I] λ6300 mentioned above. The velocities and the profiles are similar (Fig. 12, *lower panel*). That being so, it suggests that we are seeing two components of the oxygen and magnesium mass distribution in the envelope.

We estimated the expansion velocity of the Mg nebula fitting the Mg I] λ4571 line profile. The results are plotted in the upper panel of Figure 14. We emphasize that, especially at very late phases, the fitting is not satisfactory and the values plotted are only indicative. A comparison with other SNe of similar type is interesting. The FWHM of Mg I] λ4571 in the latest spectra of the Type Ib SN 1983N (225 days; Gaskell et al. 1986) and the Type Ic SN 1996aq (270 days) was about 5000 ± 300 and 7000 ± 800 km s^{-1}, respectively. A similar value (6100 km s^{-1}) was reported by Sollerman, Leibundgut, & Spyromilio (1998) for the Type Ib SN 1996N at about 220 days. These values are to be compared with 9800 ± 500 km s^{-1} measured for the same line in SN 1998bw at 201 days past maximum. However, this value reduces to 7700 ± 800 km s^{-1} if we determine the velocity using only the red half of the profile. Thus, it seems that when account is taken of the somewhat different phases at which measurements were made for these SNe, not very significant differences are noticeable.

A similar analysis is more complicated for the [O I] doublet, because of both its complex profile (see Fig. 12) and a strong contamination by the Si II λ6355 line on the red wing at phases earlier than 3 months (see Fig. 13, *left panel*). We tried to estimate the expansion velocity of the O I nebula using the blue wing of the observed profile and hence computing the FWHM of the λ6300 component alone. The results are plotted in the upper panel of Figure 14, which shows that the velocities are similar to those computed from Mg I].

Finally, we have measured the flux of the Mg I] and [O I] lines to look for possible deviations from exponential decay. The results are plotted in the lower panel of Figure 14, where it appears clearly that at late phases the flux in these lines decreases exponentially. The measured decline rates are 0.0185 and 0.0170 mag day^{-1} for the two features, respectively. These values are quite similar to those measured for the broadband photometry (see § 8). It should be noted here that Si II λ6355 line emission probably dominates the [O I] λλ6300, 6364 lines up to day 94, although there is the possibility that if [O I] is optically thick and the expansion velocities significantly exceed the doublet separation, most of the [O I] photons would be redshifted and confused with those belonging to the Si II λ6355 transition.

The unidentified blueshifted component of Mg I] will clearly dominate the photometry of this feature prior to day 125 and still contribute afterwards. The fact that Mg I] appears to reach the exponential decay line before [O I] (see Fig. 14, *lower panel*) could be due to the nature of these blending effects. Also, other considerations may be important, such as the fact that the critical density for Mg I] is 3 orders of magnitude higher than that for [O I] and the expanding envelope results in the former critical density being reached well before the latter. Also, since Mg I has a much lower ionization energy than O I, emission of these different lines may be coming from different regions. Finally, models of massive stars (Woosley, Langer, & Weaver 1995) show that magnesium occupies a more con-

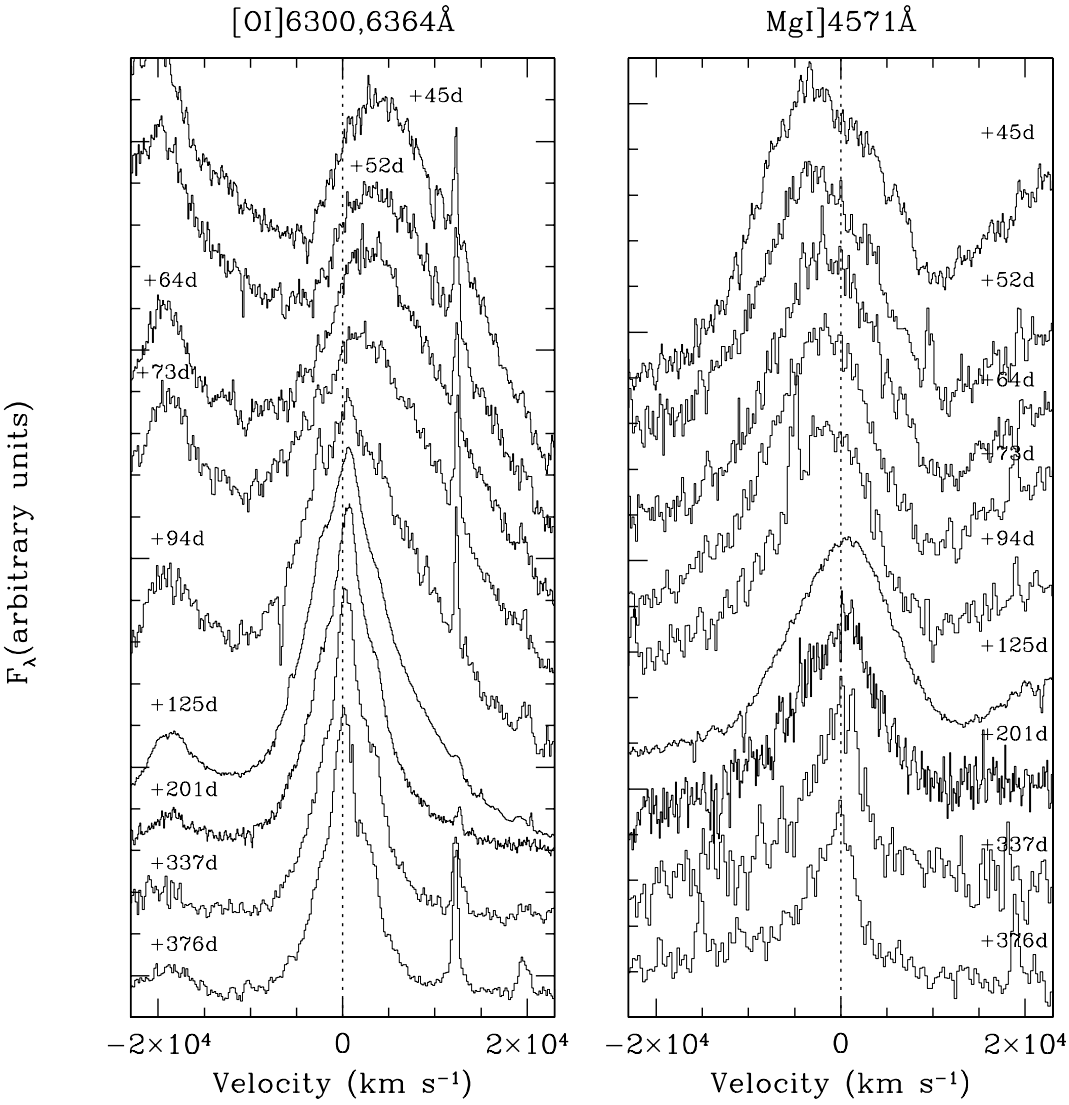

FIG. 13.—Evolution of Mg I] λ4571 (*right panel*) and [O I] $\lambda\lambda$6300, 6364 (*left panel*) line profiles

fined radial distribution than oxygen. This is the case not only for extremely massive stars but also for 13–15 $M_\odot$ stars (see Fig. 1 of Nomoto, Iwamoto, & Suzuki 1995). In both circumstances, the region where O exists without Mg is mostly He rich, the He mass fraction being ~ 0.1.

Unfortunately, it is not possible to make a similar analysis for the presumed Fe lines and particularly the feature near 5215 Å. In fact, even the identification of this feature is in doubt. One promising possibility is that it is due to the [Fe II] multiplet 19 with additional components due to the [Fe II] multiplets 16, 17, and 18. The [Fe II] multiplet 6 may then contribute to the blend near Mg I] λ4571. Nevertheless, there is no unequivocal evidence for the presence of other multiplets of [Fe II]. Another possibility suggested by Filippenko et al. (1990) for SN 1985F and SN 1987M is a combination of Fe II multiplets 35, 42, and 49. Contributions from [Fe III] multiplet 1 seems a more remote possibility because some important lines are not present. What we can state here is that the most prominent feature, the one at 5215 Å, declines faster than those of Mg I] and [O I]. The flux measurement is strongly hampered by the uncertain position of the continuum and the possible presence of another feature in the red wing (see Fig. 10). To reduce the effect of these problems, we computed the fluxes by integrating the spectra in the range 5080–5680 Å and crudely assuming the continuum level. To estimate the uncertainty involved, we chose the continuum at two extreme positions. One is the average value in the range 5680–5700 Å, where the flux drops to a minimum value, and the other is the level used in computing the flux of the Mg I] λ4571 measurements.

The results are shown in the lower panel of Figure 14, where the upper and lower extremes of the error bars represent the values obtained using the low and high continua, respectively. The conclusion is that the λ5215 feature fades at a rate of 0.021 ± 0.001 mag day^{-1}, i.e., 0.0025 ± 0.001 and 0.004 ± 0.001 mag day^{-1} faster than [O I] and Mg I], respectively. The faster decline of λ5215 is also clearly visible, if one compares its intensity to the one of the adjacent Mg I] λ4571 after normalization to its peak (see Fig. 15). This fact might also suggest that the λ5215 feature does not trace the bulk of the Fe in the envelope since one would expect the abundance of Fe to be increasing with time as a result of the radioactive decay of ^{56}Co. This might be partially compensated by the decreasing temperature and density of the ejecta.

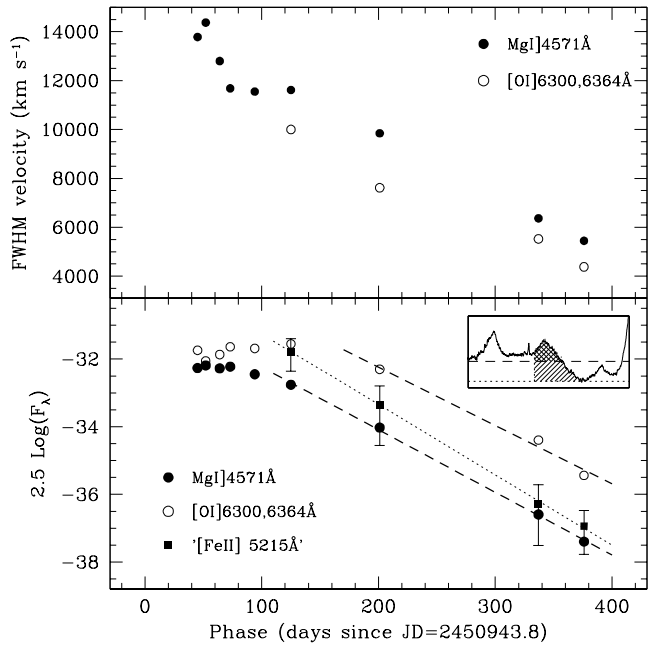

FIG. 14.—*Upper panel*: FWHM expansion velocity deduced for Mg I] λ4571 and [O I] λλ6300, 6364. *Lower panel*: Evolution of line luminosities. Dotted and dashed lines represent linear fittings to the data; line lengths indicate the phase range that has been used for the linear regression. The box in the upper right corner of the lower panel shows the region where the flux for [Fe II] λ5215 has been estimated and the position of the two continuum levels (*dashed and dotted lines*). See text for more details.

Another point concerns the expansion velocity deduced from this feature. Again the measured values are quite uncertain, but at day 201 the FWHM velocity is about 10,900 km s^{-1} and hence higher than those estimated for Mg I] λ4571 (9800 km s^{-1}) and [O I] λλ6300, 6364 (7600 km s^{-1}). However, if the λ5215 feature results from a blend of multiplet lines of whichever type, this would most certainly lead to an overestimate of the expansion velocity since the separation of individual lines of the most likely multiplets is of the order of thousands of kilometers per second. Here we only note that recent *Chandra* X-ray observations of Cas A, which is consistent with the remnant of a massive star explosion (e.g., Fesen, Becker, & Blair 1987), show that significant amounts of Fe are present at high velocities, comparable to those of lighter elements such as oxygen (Hughes et al. 2000). This implies that a relevant fraction of the material synthesized in the core has mixed into the outer regions during the SN explosion.

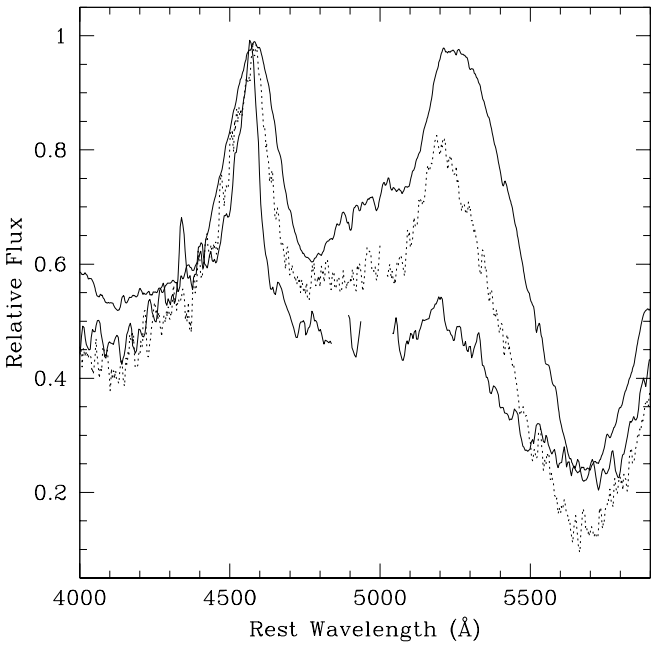

FIG. 15.—Region of Mg I] and [Fe II] at 125, 201, and 376 days (*from top to bottom*). The spectra have been normalized to the Mg I] λ4571 line peak. For presentation, the narrow emission lines emitted by the underlying H II region in the range 4800–5000 Å have been cut out, and the spectra have been smoothed using a 20 Å–wide boxcar filter.

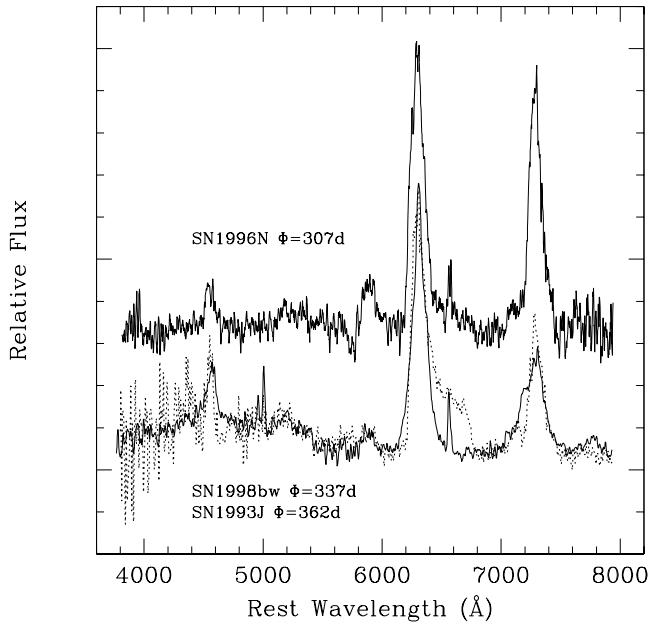

FIG. 16.—Comparison between Type IIb SN 1993J (Barbon et al. 1995; *dotted line*), Type Ib SN 1996N (Sollerman et al. 1998), and SN 1998bw at about 1 yr after maximum light. Spectra have been normalized to the [O I] λλ6300, 6364 peak and arbitrarily shifted for presentation.

Finally, we have compared SN 1998bw with the Type IIb SN 1993J and the Type Ib SN 1996N at about 1 yr after maximum light (Fig. 16). The resemblance of the three objects is evident. In particular, SN 1993J and SN 1998bw are strikingly similar, the only deviation being the broad Hα, which is missing in SN 1998bw; apart from this, line ratios and expansion velocities are definitely comparable. SN 1996N also has very similar line widths, while the luminosity ratio between [O I] and all other features is smaller and the blue [Fe II] bump is less pronounced.

Despite the great peculiarity shown in the early phases, at 1 yr after maximum SN 1998bw is spectroscopically indistinguishable from known Type Ib SNe. Even the high expansion velocities measured during the first 6 months have slowed down to the values that are typical for other Type Ib SNe (∼5000 km s^{-1}). But, the much higher ejected mass estimated by the models and the high luminosity, which persists also at these advanced phases (see next section), confirm that this event was hyperenergetic.

8. BROADBAND AND BOLOMETRIC LIGHT CURVES

The photometric data presented in this paper and those published by Galama et al. (1998a), McKenzie & Schaefer (1999), and Sollerman et al. (2000) can be collected in a

unique data set to study the late-phase behavior of the light curves, as shown in Figure 17. This figure shows that the SN luminosity follows an exponential luminosity decline up to about 300 days after maximum light, while a clear flattening is present for the latest observed epochs, especially in the V band. This is clearly shown in Table 4, where we have reported the decay rates computed via linear least-squares fit to the data in the two phase ranges 40–330 and 300–490 days from B maximum. The values for the earliest data are consistent, within the estimated errors, with those computed by McKenzie & Schaefer (1999) using data in the range 47–171 days ($\gamma_B = 0.0141 \pm 0.0002$, $\gamma_V = 0.0184 \pm 0.0002$, and $\gamma_I = 0.0181 \pm 0.0002$ mag day^{-1}).

In any case, these slopes deviate clearly from the values expected from the $^{56}\mathrm{Co} \rightarrow {}^{56}\mathrm{Fe}$ radioactive decay in the case of complete γ-ray trapping (0.0098 mag day^{-1}), as already noticed by McKenzie & Schaefer (1999). On the other hand, the measured slopes are similar to those reported by Sollerman et al. (1998) for the Type Ib SN 1996N in the phase range 180–340 days ($\gamma_V = 0.0167 \pm 0.0023$, $\gamma_R = 0.0172 \pm 0.0010$, and $\gamma_I = 0.0193 \pm 0.0024$ mag day^{-1}). These values are even higher than those typical for the late-phase data of Type Ia SNe. If ^{56}Co decay is powering the late light curve of SN 1998bw, there must be a fairly strong leakage in the γ-ray deposition, as for SN 1996N (Sollerman et al. 1998). Interestingly, fast and slow decliners seem to exist within the Type Ic class, as pointed out by Clocchiatti & Wheeler (1997). The range spanned by late-phase decline rates of SNe Ib/c is quite broad: γ_B ranges from 0.006 (SN 1990B; Piemonte 2001) to 0.022 mag day^{-1} (SN 1990I; ESO-KP database). At later phases ($t \geq 300$ days), a clear flattening of the light curve is visible in all passbands, even though the conclusion about B band is somewhat hampered by the lack of data at phases later than 403 days. The decline rate variation is 0.0020 ± 0.0013, 0.0079 ± 0.0010, 0.0036 ± 0.0020, and 0.0043 ± 0.0013 mag day^{-1} in B, V, R, and I, respectively.

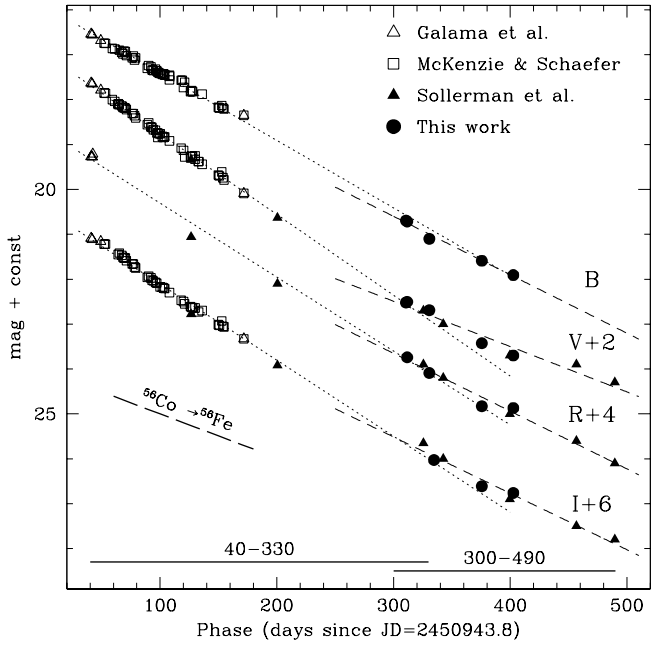

FIG. 17.—*BVRI* broadband light curves of SN 1998bw at $t > 40$ days. For presentation the light curves have been shifted by the reported amounts. No extinction correction has been applied. The dotted and dashed lines represent least-squares fittings to the data in the ranges 40–330 and 300–490 days past B maximum. Data are from Galama et al. (1998a), McKenzie & Schaefer (1999), Sollerman et al. (2000), and this work. The thick dashed line corresponds to the $^{56}\mathrm{Co} \rightarrow {}^{56}\mathrm{Fe}$ decay rate, expected for full γ-ray trapping. Epochs refer to the B maximum light.

In Figure 18, we present the UVOIR bolometric light curve of SN 1998bw, which was constructed using all available data by integrating the flux in the optical and near-IR photometric bands. Magnitudes were converted to fluxes using the calibrations of Bessell (1979) and Wilson et al. (1972). The measured fluxes were then transformed to luminosities by adopting a distance modulus $\mu = 32.89$ ($d = 37.8$ Mpc; $H_0 = 65$ km s^{-1} Mpc^{-1}) and an extinction $A_V = 0.2$. We emphasize that JHK photometry is available only for the early phases and that its contribution to the total flux is quite significant, ranging from $\sim$25% on day 22.4 (from GRB) to $\sim$35% on day 65.4. For later epochs we simply assume that the fractional IR contribution remained constant at 35% as for the last measurement. Clearly, this is a major source of uncertainty for the late UVOIR bolometric light curve.

After the maximum peak, where the SN reaches a luminosity of $\sim 10^{43}$ ergs s^{-1}, the light curve settles on the exponential decay tail starting with day +40, with a decline rate $\gamma = 0.0176 \pm 0.0002$ mag day^{-1}. Then, after day +300, the bolometric light curve appears to flatten, gradually deviating from the slope defined by the data in the range 40–200 days (*dotted line*), so that at +490 days the difference is about 1.4 mag, which is well outside the error bars (see Fig. 18). These uncertainties were estimated taking into account the presence of possible contamination from the unresolved underlying H II region, whose contribution is difficult to subtract (see below).

The comparison of the bolometric light curve of SN 1998bw with the model of Iwamoto et al. (1998) is also

TABLE 4

DECLINE RATES OF SN 1998bw IN THE PHASE RANGES 40–330 AND 300–490 DAYS FROM B MAXIMUM

Parameter	B	V	R	I
Phase range[a]	40.8–311.6	40.8–325.6	40.8–325.6	40.8–325.6
Number of points.....	51	57	7	47
γ (mag day^{-1})	0.0150 ± 0.0010	0.0180 ± 0.0006	0.0165 ± 0.0019	0.0169 ± 0.0010
Phase range[a]	310.6–402.6	310.6–489.6	311.6–489.6	325.6–489.6
Number of points.....	5	10	9	8
γ (mag day^{-1})	0.0130 ± 0.0008	0.0101 ± 0.0008	0.0129 ± 0.0006	0.0126 ± 0.0008

[a] Relative to B maximum (JD = 2,450,943.8).

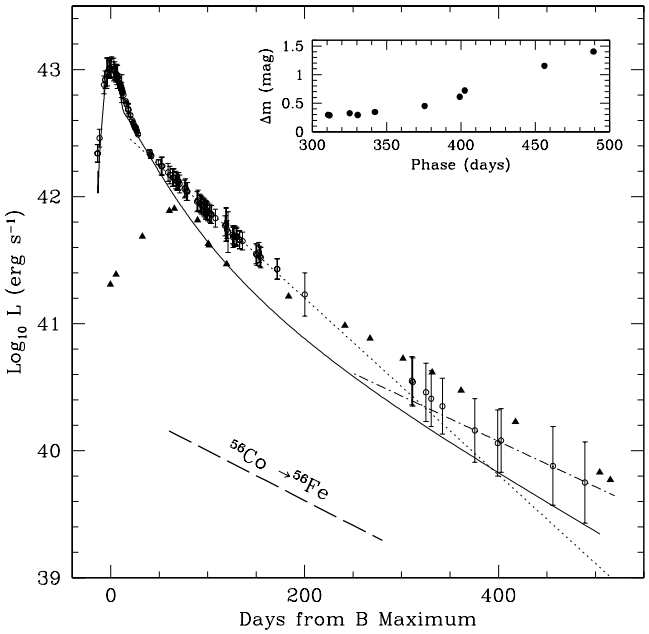

FIG. 18.—Comparison between the UVOIR bolometric light curve of SN 1998bw and the hypernova model by Iwamoto et al. (1998; *solid line*). The dotted line represents an extrapolation of a least-squares fit to the data in the range 50–200 days, while the dot-dashed line is a fit to the data in the phase range 376–490 days. The dashed line corresponds to the $^{56}Co \rightarrow {}^{56}Fe$ decay rate, expected for full γ-ray trapping. The plot in the upper right part of the figure shows the deviations of the observed data from the extrapolation on the early light curve (50–200 days; see text). For comparison, the bolometric light curve of SN 1987A (Bouchet, Danziger, & Lucy 1991) is also plotted (*filled triangles*).

presented in Figure 18. Although the early phases ($t \leq 60$ days) are well reproduced, the observed tail deviates from the theoretical prediction. The model must be highly energetic to accommodate the early light curve and spectra. Therefore, at later phases γ-rays should escape quite efficiently, resulting in a rapid decline. Eventually, most γ-rays escape from the ejecta, and only positrons from the ^{56}Co decay contribute to the light curve (the masses of ^{57}Co and ^{44}Ti in the model are small). Indeed, after day $\sim$200 the calculated decline becomes slower, and it approaches the decay rate of ^{56}Co around day 400 (Iwamoto et al. 1998; Nakamura et al. 1999, 2000, 2001).

Nomoto et al. (2001) and Nakamura et al. (2001) have shown that, while the highly energetic model can explain the early light curve, a less energetic model is in better agreement with the late light curve. They suggest that such a behavior reflects some nonspherical effects in the ejecta structure, although the well-mixed models of Sollerman et al. (2000) do not require asymmetries for a reasonable match to the light curves and neither do those of Chugai (2000).

Jeffery's (1999) ad hoc model, although based on a rather different model of the ejecta, also predicts that the pure exponential phase should end after about day 400 and that the light curve should slowly approach the ^{56}Co decay slope when eventually only the positrons are deposited (provided that other, less abundant radioactive species remain unimportant and interaction with circumstellar material does not occur). In this respect it is interesting to note that a least-squares fit to the bolometric light curve in the phase range 376–490 days gives a slope $\gamma = 0.009 \pm 0.001$ mag day^{-1}, which would suggest that SN 1998bw finally settled on the ^{56}Co decay. Nevertheless, a possible alternative is that the flattening is due to the unaccounted presence of other sources within the ground-based point-spread function. In order to reproduce the observed behavior, the integrated magnitude of the contaminating objects must be $V \sim 22.6$. Even though recent *HST* Space Telescope Imaging Spectrograph (STIS) observations (Fynbo et al. 2000) have shown that several objects are present within a radius of 0.″5 from the SN location (Fig. 1), there is no evidence for such a relatively bright source. Hence, the conclusion is that the observed flattening is, at least to some extent, intrinsic. However, this can only be confirmed by follow-up observations by *HST*. On the other hand, the effects of possible freeze-out, ejecta-wind interaction, or even faint echoes should not be overlooked.

As a matter of fact, no signs of ejecta-wind interaction are found in the late-phase spectra of SN 1998bw (see also Sollerman et al. 2000). Nevertheless, some circumstellar material (CSM) is expected to be present. All models for SNe Ic assume that the progenitor stars undergo intense mass loss and lose their H-He envelopes to become bare CO cores before they explode. Thus, interaction should be expected at some stage. Future observations will be fundamental to investigate the circumstellar environment and the real onset of ejecta-wind interaction.

In Figure 19 the absolute V light curve of SN 1998bw is presented and compared with the light curves of some Type II (1987A, 1979C), IIb (1993J), Ia (1991T, 1992A), Ib (1990I), and Ic (1992ar, 1994I) SNe. For SN 1998bw, a distance

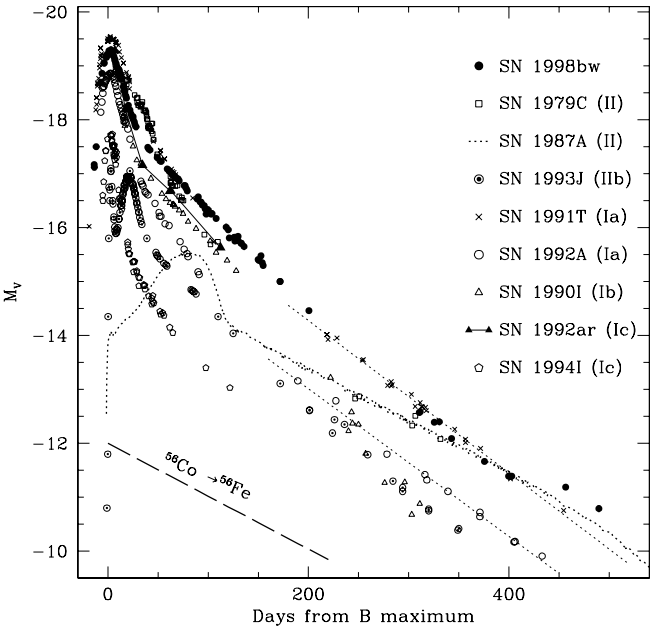

FIG. 19.—Absolute V light curve of SN 1998bw compared with SNe 1987A, 1979C (Balinskaya et al. 1980; de Vaucouleurs et al. 1981; Barbon et al. 1982), 1993J (IAU Circulars; Lewis et al. 1994; Barbon et al. 1995), 1991T (Phillips et al. 1992; Cappellaro et al. 1997), 1992A (Suntzeff 1996; Cappellaro et al. 1997), 1990I (ESO-KP database, unpublished), 1992ar (Clocchiatti et al. 2000), and 1994I (Tsvetkov & Pavlyuk 1995; Richmond et al. 1996). Note that for SN 1992ar the brightest case was chosen (see Clocchiatti et al. 2000). The dotted lines represent a least-squares fit to the late-phase data of SNe 1991T and 1992A. The dashed line corresponds to the $^{56}Co \rightarrow {}^{56}Fe$ decay rate, expected for full γ-ray trapping.

modulus $\mu = 32.89$, while the interstellar extinction is assumed to be $A_V = 0.2$ mag (see § 5). It is clear that the light curve alone would not allow one to classify this object as an SN Ib/c nor, indeed, to distinguish it from thermonuclear SNe.

Even though the internal extinction for SN 1994I is very uncertain (here we adopted $A_V = 1.2$), SN 1998bw was much brighter and had a different light curve shape. Unfortunately, late-phase data for SN 1994I are not available. However, a comparison is possible with the Type Ib SN 1990I. Maximum light was not covered by the observations, but the light curve of SN 1990I between day +40 and day +120 is very similar to that of SN 1998bw, although about 0.5 mag fainter. After that the luminosity decay rate of SN 1990I was larger than that of SN 1998bw. Later on, the overluminosity of this SN becomes more pronounced. At 350 days the Type IIb SN 1993J is 1.4 mag fainter then SN 1998bw (see Fig. 19). SN 1996N is even less luminous as shown by Sollerman et al. (1998), even though the distance modulus, reddening, and epoch of maximum are rather uncertain. One year after the explosion, this SN is about 3 mag fainter than SN 1998bw.

As discussed before, we believe that the late-time light curve of SN 1998bw is powered by the radioactive decay of ^{56}Co into ^{56}Fe and therefore the late luminosity can be used to constrain the ^{56}Ni mass ejected by the explosion. The decay of $^{56}\mathrm{Co} \rightarrow {}^{56}\mathrm{Fe}$ releases energy through the γ-ray channel in 81% of the cases, while the remaining fraction goes into positrons, which annihilate with electrons producing γ-rays (see Colgate & McKee 1969). The positron kinetic energy released before the annihilation accounts for 3.5% of the total ^{56}Co decay energy (Arnett 1979; Woosley, Pinto, & Hartmann 1989).

In the case of SN 1998bw, since the slope of the late light curve prior to 300 days is steeper than the expected input energy from ^{56}Co decay, we can assume that in this phase range some fraction of the γ-rays escapes thermalization. At later epochs ($t > 400$ days), the envelope becomes completely transparent to γ-rays, whereupon in the case of complete deposition of positron kinetic energy (Axelrod 1980), the late light curve settles on the ^{56}Co decay line.

Making the crude assumption that the phase of complete escape of γ-rays and complete deposition of positrons was reached after 400 days and assuming a rate of ^{56}Co decay energy production of $s = 6.78 \times 10^9$ ergs g^{-1} s^{-1} (Sutherland & Wheeler 1984) and a half-life time of 77.12 days (Arnett 1996, p. 428), we can estimate the mass of $M(^{56}\mathrm{Ni})$ using the following equation:

$$M(^{56}\mathrm{Ni}) \lesssim \frac{\mathrm{L}_{43}(t)}{1.35e^{-t/111.26} \times 0.035} \; M_\odot \,, \qquad (1)$$

where $L_{43}(t)$ is the bolometric luminosity in 10^{43} ergs s^{-1}, t is expressed in days from the explosion, and the factor 0.035 is the fraction of total ^{56}Co decay energy deposited by positrons. If we use the four available measurements at $t > 400$ days (Sollerman et al. 2000; this work) and average the results, we get $M(^{56}\mathrm{Ni}) \leq 1.0^{+0.5}_{-0.2}\ M_\odot$. The errors are by far dominated by the uncertainties in the bolometric luminosities, and the estimate depends on our assumption on the IR contribution at these late phases.

We note that the model by Nakamura et al. (2001) estimated the mass of ^{56}Ni to be 0.4 $M_\odot$ from the early light curve modeling. This value is not in contradiction with what is found here if the SN envelope is not completely transparent to γ-rays at $t > 400$ days. Moreover, it must be noted that Nakamura et al. (2001) have suggested that positron contribution is not yet dominant in powering the light curve at the phases covered by the last available observations.

9. DISCUSSION AND CONCLUSIONS

As we have shown, SN 1998bw was exceptional in many respects, even beyond its possible and probable connection with GRB 980425. The luminosity at maximum was comparable to that of an SN Ia, but its spectral appearance was completely different from that class of objects. On the other hand, while the Type Ic classification at maximum holds by definition (no H or He, weak Si II), SN 1998bw had little in common with objects previously classified as Type Ib or Ic (see also Stathakis et al. 2000), at least around maximum. Among all studied Type Ib/c SNe, only SN 1992ar might have been brighter than SN 1998bw (Clocchiatti et al. 2000). The only known SNe that bear some spectroscopic resemblance to this unusual object are SN 1997ef (Garnavich et al. 1997) and SN 1998ey (Garnavich, Jha, & Kirshner 1998), the former also being possibly associated with a GRB (Wang & Wheeler 1998). Even so, SN 1997ef was fainter than SN 1998bw and probably produced much less ^{56}Ni than SN 1998bw (Iwamoto et al. 1998, 2000). It must be mentioned here that SN 1997cy, also conceivably but by no means certainly associated with a GRB (Woosley et al. 1999; Germany et al. 2000), was extremely bright, probably the brightest SN ever observed, but it has shown signs of ejecta-CSM interaction at all epochs (Turatto et al. 2000).

The deviation from any known Type Ib SN behavior is also noticeable in the early nebular phase, when the spectrum of SN 1998bw is probably dominated by Fe blends in the blue and by O and Ca in the red, as already pointed out by Patat & Piemonte (1998b). A somewhat similar behavior was noticed in SN 1993R by Ruiz-Lapuente (see Filippenko 1997a) and in SN 1990aj by Piemonte (2001).

The high velocities and the large intrinsic luminosity suggest that SN 1998bw was produced by an extremely energetic explosion. All published models reach this conclusion, even if the explosion energy, the progenitor mass, and ejected ^{56}Ni mass span quite a wide range (Iwamoto et al. 1998; Höflich et al. 1999; Woosley et al. 1999; Nakamura et al. 2001). This range arises because different degrees of asymmetry and beaming have been used. The exceptionally high value of the kinetic energy of the models that give the best fit to both the light curve and the spectra of SN 1998bw (3.0×10^{52} ergs, Iwamoto et al. 1998; 5.7×10^{52} ergs, Nakamura et al. 2000, 2001; 6.0×10^{52} ergs, Branch 2001) led to the designation of this object as a hypernova, even though it does not match the original hypernova definition (Paczyński 1998).

Despite the great individuality shown by SN 1998bw at maximum light, 1 yr later its spectrum is very similar to that of other Type Ib/c events. This gives qualitative support to the idea that the material ejected by SN 1998bw was rich in both Fe-peak and α-elements. The possibly large production of Fe-peak elements makes it important to obtain detailed nucleosynthesis calculations and rate estimates of the occurrence of such objects, because they might have a significant impact on models of galactic chemical evolution. Since SN 1998bw was as bright as an SN Ia, it might seem

unlikely that such objects would be missed in nearby searches. Nevertheless, SN 1998bw may have been missed had there not been an associated GRB. Does this allow us to infer that such kinds of explosions must be intrinsically rare at the present epoch?

But, even if they are relatively rare now, their past frequency may have been considerably higher. SN 1998bw is thought to have been generated by a massive star (see Iwamoto et al. 1998; Woosley et al. 1999), which may have been more common at remote epochs, when the rate of star formation was higher. Since the timescale for the release of iron and oxygen into the interstellar medium by these objects is much shorter than for SNe Ia and significantly less massive core-collapse SNe, hypernovae may have played an important role in the initial galactic chemical enrichment. Future work will concentrate on establishing whether the rate of occurrence of such SNe increases with redshift or look-back time. It is possible that the discovery of many GRBs at significant redshift is already a hint in this direction, as is the conclusion for several of them that the light curve can be reproduced with a combination of a GRB afterglow plus an SN light curve (see Bloom et al. 1999).

This work is based on data collected at ESO–La Silla. We express our gratitude to the Visiting Astronomers who kindly gave us part of their observing time in order to secure a good follow-up of this important object. In particular, we acknowledge the support we received from Pierre Leisy and Alessandro Pizzella during the observations at La Silla. We finally wish to thank Stephen Holland and Jens Hjorth for making the *HST*-STIS image of SN 1998bw available to us.

This work has been partially supported by grants-in-aid for scientific research (07CE2002, 12640233) from the Ministry of Education, Science, Culture, and Sports of Japan. The authors made use of the NASA/IPAC Extragalactic Database (NED), which is operated by the Jet Propulsion Laboratory, California Institute of Technology, under contract with the National Aeronautics and Space Administration.

REFERENCES

Arnett, W. D. 1979, ApJ, 230, L37
———. 1996, Supernovae and Nucleosynthesis (Princeton: Princeton Univ. Press)
Axelrod, T. S. 1980, Ph.D. thesis, Univ. California, Santa Cruz
Balinskaya, I. S., et al. 1980, A&A, 85, L19
Barbon, R., Benetti, S., Cappellaro, E., Patat, F., Turatto, M., & Iijima, T. 1995, A&AS, 110, 513
Barbon, R., et al. 1982, A&A, 116, 43
Bessell, M. S. 1979, PASP, 91, 589
———. 1990, PASP, 102, 1181
Bessell, M. S., & Brett, J. M. 1988, PASP, 100, 1134
Bloom, J. S., et al. 1999, Nature, 401, 453
Bouchet, P., Danziger, I. J., & Lucy, L. B. 1991, AJ, 102, 1135
Branch, D. 2001, in Supernovae & Gamma-Ray Bursts, ed. M. Livio, N. Panagia, & K. Sahu (STScI Symp. Ser. 13; Cambridge: Cambridge Univ. Press)
Burstein, D., & Heiles, C. 1982, AJ, 87, 1165
Cappellaro, E., Mazzali, P., Benetti, S., Danziger, I. J., Turatto, M., della Valle, M., & Patat, F. 1997, A&A, 328, 203
Chugai, N. N. 1987, Soviet Astron. Lett., 13, 282
———. 2000, Astron. Lett., 26, 797
Clocchiatti, A., et al. 1996, ApJ, 462, 462
———. 2000, ApJ, 529, 661
Clocchiatti, A., Phillips, M., Spyromilio, J., & Leibundgut, B. 2001, in SN 1987A: Ten Years After: Fifth CTIO/ESO/LCO Workshop, ed. M. M. Phillips & N. B. Suntzeff, in press
Clocchiatti, A., & Wheeler, J. C. 1997, in Thermonuclear Supernovae, ed. P. R. Lapuente, R. Canal, & J. Isern (NATO ASI Ser. C, 486; Dordrecht: Kluwer), 863
Colgate, S. A., & McKee, C. 1969, ApJ, 157, 623
de Vaucouleurs, G., de Vaucouleurs, A., Corwin, H. G., Jr., Buta, R. J., Paturel, G., & Fouque, P. 1991, Third Reference Catalogue of Bright Galaxies (Version 3.9; New York: Springer)
de Vaucouleurs, G., et al. 1981, PASP, 93, 36
Fesen, R. A., Becker, R. H., & Blair, W. P. 1987, ApJ, 313, 378
Filippenko, A. V. 1997a, in Thermonuclear Supernovae, ed. P. R. Lapuente, R. Canal, & J. Isern (NATO ASI Ser. C, 486; Dordrecht: Kluwer), 795
———. 1997b, IAU Circ. 6783
———. 1998, IAU Circ. 6969
Filippenko, A. V., et al. 1995, ApJ, 450, L11
Filippenko, A. V., Porter, A. C., & Sargent, W. L. W. 1990, AJ, 100, 1575
Fynbo, J. U., et al. 2000, ApJ, 542, L89
Galama, T. J., et al. 1998a, Nature, 395, 670
Galama, T. J., Vreeswijk, P. M., Pian, E., Frontera, F., Doublier, V., & Gonzalez, J. F. 1998b, IAU Circ. 6895
Garnavich, P. M., Jha, S., & Kirshner, R. P. 1998, IAU Circ. 7066
Garnavich, P. M., Jha, S., Kirshner, R. P., Challis, P. M., Balam, D., Brown, W., & Briceno, C. 1997, IAU Circ. 6786
Gaskell, C. M., Cappellaro, E., Dinerstein, H. L., Harkness, R. P., & Wheeler, J. C. 1986, ApJ, 306, L77
Gerardy, C. L., Fesen, R. A., Höflich, P., & Wheeler, J. C. 2000, AJ, 119, 2968
Germany, L. M., Reiss, D. J., Schmidt, B. P., Stubbs, C. W., & Sadler, E. M. 2000, ApJ, 533, 320
Graham, J. R. 1988, ApJ, 335, L53
Hamuy, M., Walker, A. R., Suntzeff, N. B., Gigoux, P., Heathcote, S. R., & Phillips, M. M. 1992, PASP, 104, 533
Harkness, R. P., et al. 1987, ApJ, 317, 355
Höflich, P. 1995, ApJ, 443, 89
Höflich, P., Wheeler, J. C., & Wang, L. 1999, ApJ, 521, 179
Hughes, J. P., Rakowski, C. E., Burrows, D. N., & Slane, P. O. 2000, ApJ, 528, L109
Iwamoto, K., et al. 1998, Nature, 395, 672
———. 2000, ApJ, 534, 660
Jeffery, D. J. 1999, preprint (astro-ph/9907015)
Jeffery, D. J., & Branch, D. 1990, in Supernovae, ed. J. C. Wheeler, T. Piran, & S. Weinberg (Singapore: World Scientific), 149
Kay, L. E., Halpern, J. P., Leighly, K. M., Heathcote, S., & Magalhaes, A. M. 1998, IAU Circ. 6969
Kulkarni, S. R., et al. 1998, Nature, 395, 663
Landolt, A. U. 1992, AJ, 104, 340
Lewis, J. R., et al. 1994, MNRAS, 266, L27
Lidman, C., Doublier, V., Gonzalez, J. F., Augusteijn, T., Hainaut, O., Boehnhardt, H., Patat, F., & Leibundgut, B. 1998, IAU Circ. 6895
Lucy, L. B. 1991, ApJ, 383, 308
Maeda, K., Nakamura, T., Nomoto, K., Mazzali, P. A., Patat, F., & Hachisu, I. 2000, ApJ, submitted (astro-ph/0011003)
Martin, W. C. 1987, Phys. Rev. A, 36, 3575
Mazzali, P. A. 2000, A&A, 363, 705
Mazzali, P. A., Iwamoto, K., & Nomoto, K. 2000, ApJ, 545, 407
Mazzali, P. A., & Lucy, L. B. 1998, MNRAS, 295, 428
McGregor, P. 1995, CASPIR User's Manual (Mount Stromlo and Siding Spring Observatories)
McKenzie, E. H., & Schaefer, B. E. 1999, PASP, 111, 964
Meikle, W. P. S., Allen, D. A., Spyromilio, J., & Varani, G. F. 1989, MNRAS, 238, 193
Millard, J., et al. 1999, ApJ, 527, 746
Nakamura, T., et al. 2000, in IAU Symp. 195, Highly Physical Processes and Mechanisms for Emission from Astrophysical Plasmas, ed. P. C. H. Martens, S. Tsuruta, & M. Weber (San Francisco: ASP), 347
Nakamura, T., Mazzali, P. A., Nomoto, K., & Iwamoto, K. 2001, ApJ, 550, 991
Nakamura, T., Mazzali, P. A., Nomoto, K., Iwamoto, K., & Umeda, H. 1999, Astron. Nachr., 320, 363
Nomoto, K., et al. 2001, in Supernovae & Gamma-Ray Bursts, ed. M. Livio, N. Panagia, & K. Sahu (STScI Symp. Ser. 13; Cambridge: Cambridge Univ. Press)
Nomoto, K., Iwamoto, K., Nakasato, N., Thielemann, F.-K., Brachwitz, F., Tsujimoto, T., Kubo, Y., & Kishimoto, N. 1997, Nucl. Phys. A, 621, 467c
Nomoto, K., Iwamoto, K., & Suzuki, T. 1995, Phys. Rep., 256, 173
Oke, J. B. 1990, AJ, 99, 1621
Paczyński, B. 1998, ApJ, 494, L45
Patat, F. 1996, Ph.D. thesis, Univ. Padova
———. 1999, EFOSC2 User's Manual (LSO-MAN-ESO-36100-0004)
Patat, F., Barbon, R., Cappellaro, E., & Turatto, M. 1994, A&A, 282, 731
Patat, F., Benetti, S., Cappellaro, E., Danziger, I. J., della Valle, M., Mazzali, P. A., & Turatto, M. 1996, MNRAS, 278, 111
Patat, F., et al. 2000, Mem. Soc. Astron. Italiana, 71(2), 307
Patat, F., & Piemonte, A. 1998a, IAU Circ. 6918
Patat, F., & Piemonte, A. 1998b, IAU Circ. 7017
Perryman, M. A. C., et al. 1997, A&A, 323, L49

Phillips, M. M., Heathcote, S. R., Hamuy, M., & Navarrete, M. 1988, AJ, 95, 1087
Phillips, M. M., Wells, L. A., Suntzeff, N. B., Hamuy, M., Leibundgut, B., Kirshner, R. P., & Foltz, C. B. 1992, AJ, 103, 1632
Pian, E., et al. 1999, A&AS, 138, 463
Piemonte, A. 2001, in SN 1987A: Ten Years After: Fifth CTIO/ESO/LCO Workshop, ed. M. M. Phillips & N. B. Suntzeff, in press
Pinto, P. A., & Eastman, R. G. 2000, ApJ, 530, 757
Richmond, M. W., et al. 1996, AJ, 111, 327
Sadler, E. M., Stathakis, R. A., Boyle, B. J., & Eckers, R. D. 1998, IAU Circ. 6901
Schlegel, D. J., Finkbeiner, D. P., & Davis, M. 1998, ApJ, 500, 525
Schmidt, B. P., et al. 1994, AJ, 107, 1444
Soffita, P., et al. 1998, IAU Circ. 6884
Sollerman, J., Leibundgut, B., & Spyromilio, J. 1998, A&A, 337, 207
Sollerman, J., Kozma, C., Fransson, C., Leibundgut, B., Lundqvist, P., Ryde, F., & Woudt, P. 2000, ApJ, 537, L127
Suntzeff, N. 1996, in IAU Colloq. 145, Supernovae and Supernova Remnants, ed. R. McCray & Z. Wang (Cambridge: Cambridge Univ. Press), 41
Sutherland, P. G., & Wheeler, J. C. 1984, ApJ, 280, 282
Stathakis, R. A., et al. 2000, MNRAS, 314, 807
Tinbergen, J., & Rutten, R. 1992, A User's Guide to WHT Spectropolarimetry (ING; La Palma User Manual No. 21)
Tinney, C., Stathakis, R., & Cannon, R. 1998, IAU Circ. 6896
Tsvetkov, D. Y., & Pavlyuk, N. N. 1995, Astron. Lett., 21, 606
Turatto, M., et al. 1990, Messenger, 60, 15
———. 2000, ApJ, 534, L57
Turnshek, D. A., Bohlin, R. C., Williamson, R. L., Lupie, O. L., & Koornneef, J. 1990, AJ, 99, 1243
Walsh, J. R. 1992, in 4th ESO/ST-ECF Data Analysis Workshop, ed. P. J. Grosbol & R. C. E. Ruijsscher (Garching: ESO), 53
Wang, L., & Wheeler, J. C. 1998, ApJ, 504, L87
Wang, L., Wheeler, J. C., Li, Z. W., & Clocchiatti, A. 1996, ApJ, 467, 435
Wheeler, J. C. 2001, in Supernovae & Gamma-Ray Bursts, ed. M. Livio, N. Panagia, & K. Sahu (STScI Symp. Ser. 13; Cambridge: Cambridge Univ. Press)
Wilson, W. J., Schwartz, P. R., Neugebauer, G., Harvey, P. M., & Becklin, E. E. 1972, ApJ, 177, 523
Woosley, S. E., Eastman, R. G., & Schmidt, B. P. 1999, ApJ, 516, 788
Woosley, S. E., Langer, N., & Weaver, T. A. 1995, ApJ, 448, 315
Woosley, S. E., Pinto, P. A., & Hartmann, D. 1989, ApJ, 346, 395